Synthesis and photoswitching properties of bioinspired dissymmetric γ-pyrone, analogue of cyclocurcumin

Jérémy Pecourneau,[a] Raúl Losantos,[a,b] Antonio Monari,[b] Stéphane Parant,[a] Andreea Pasc,[a*] Maxime Mourer[a*]

[a]Univ Lorraine, CNRS, L2CM UMR 7053, Bvd des Aiguillettes, F-54506 Vandœuvre-lès-Nancy, France

[b]Univ Lorraine, CNRS, LPCT UMR 7019, Bvd des Aiguillettes, F-54506 Vandœuvre-lès-Nancy, France

*Corresponding authors.

E-mail address: andreea.pasc@univ-lorraine.fr, maxime.mourer@univ-lorraine.fr

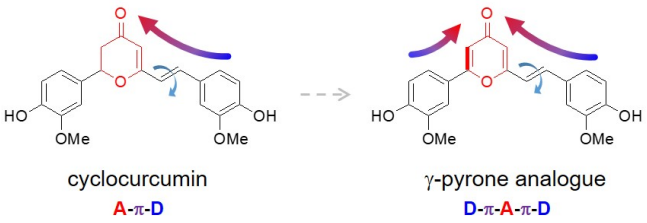

Abstract: Cyclocurcumin (CC), a turmeric curcuminoid with potential therapeutic properties, is also a natural photoswitch that may undergo *E*/*Z* photoisomerization under UV light. To be further exploited in relevant biological applications, photoactivation under near infrared (NIR) irradiation is required. Such requirement can be met through opportune chemical modifications, by favoring two-photon absorption (TPA) probability. Herein, a general and efficient synthesis of a biomimetic 2,6-disubstituted-γ-pyrone analogue of cyclocurcumin is described, motivated by the fact that molecular modeling previews an order of magnitude increase of its NIR TPA for the latter compared to CC. Three retrosynthetic pathways have been identified (i) *via* an aryl-oxazole intermediate or *via* an aryl-diynone through (ii) a bottom-up or (iii) a top-down approach. While avoiding the passage through unstable synthons or low yield intermediate reactions, only the latest approach could conveniently afford the 2,6-disubstituted-γ-pyrone analogue of cyclocurcumin, in ten steps and with an overall yield of 18%. The photophysical properties of our biomimetic analogue have also been characterized showing an improved

photo-isomerization yield over the parent natural compound. The potentially improved non-linear optical properties, as well an enhanced stability, may be correlated to the enforcement of the planarity of the pyrone moiety leading to a quadrupolar D-π-A-π-D system.

Keywords: pyrone, cyclocurcumin, biomimetic, photoswitch, two-photon absorption.

Introduction

Molecular photoswitches are compounds capable to reversibly populate, under the effect of an external perturbation such as the absorption of electromagnetic light, two different stable states, *i.e.* conformation or configuration isomers, that should ideally present significantly different geometries and photochromic properties. The capability of controlling the interconversion between the two states is clearly extremely beneficial in potentially providing molecular-based smart materials or devices, as well as molecular machines converting light energy into mechanical work.

Although, their potential is still far for being fully explored, both synthetic and natural photoswitches already found a wide range of applications, including optogenetics and imaging, biotechnology, or pharmacology.

The most well-known natural photoswitch is the chromophore of the transmembrane rhodopsin protein, *i.e.* the protonated Schiff-base of the 11-*cis* retinal, which following the absorption of visible light switches into all-*trans* retinal to initiate the cascade leading either to transmembrane ion transport in bacteria or to vision in superior animals. Most notably, rhodopsin-embedded retinal is also one of the most extremely efficient switches both considering the high quantum yield (approaching 80%) and the ultrafast reaction (around 120 fs). The molecular and photochemical bases, in terms of the topology of the involved potential energy surfaces (PES) at the base of such efficiency have been deeply characterized by both time-resolved spectroscopy and computational photochemistry,[1] while recently possible dark-photochemistry based isomerization related to photodynamic therapy side effects have also been unraveled.[2] The combined use of biomimetic strategy and the opportune molecular design is clearly beneficial in improving photoswitching capabilities.[3] Several other molecular photoswitches have been reported to date, *i.e.* 9-aryl-phenalenones whose photocyclization is the key step in the defense mechanism of plants against pathogens[4] or flavylium derivatives, bioinspired from anthocyanins, the natural colorants of most red and blue flowers and fruits.[5]

Herein, we report the first bioinspired photoswitch derived from cyclocurcumin (CC). As a matter of fact, CC is a natural compound (Scheme 1), that can be isolated in small amount from turmeric rhizome (*Curcuma longa*). Despite the fact that the remarkable potential pharmacological properties of curcumin are by far driving the most interest, more recent studies revealed the antioxidant, anti-vasoconstrictive, immune-modulating, and neuroprotective effects of cyclocurcumin. However, photoswitching properties of cyclocurcumin were only scarcely investigated, even though they have been demonstrated and rationalized computationally, together with their dependence on the environmental factors.[6]

Cyclocurcumin has an α,β-unsaturated dihydropyrone moiety that allows the *trans-cis* photoisomerization of the β ethylenic bound (Scheme 1).[7] The predominant form of CC both in natural compounds and in solution is the *trans* isomer which is thermodynamically most favorable. Direct *trans-cis* isomerization of CC occurs under irradiation at around λ_{max} = 375 nm while the reverse reaction takes place thermally or photochemically following the exposure to 300 nm light. CC also exhibits fluorescence emission at around 500 nm, as a function of the solvent. Interestingly, molecular modeling suggests that the competition between the two excited-state relaxation routes, photoisomerization *vs* fluorescence, is strongly dependent on the polarity of the environment, which ultimately determines the observed outcome.[6] The competition between the two processes, especially in complex and inhomogeneous biological environments, is detrimental to achieve an exploitable quantum yield. Indeed, an ideal molecular photoswitch should be chemically stable, should have a high photoisomerization yield, large spectral differences between the isomers, and low fatigue, *i.e.* the ability of optical resetting.

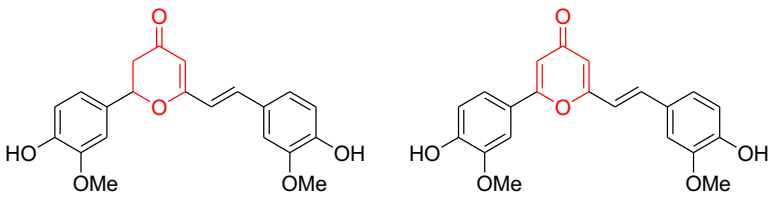

Scheme 1. Natural cyclocurcumin and its 2,6-disubstituted-γ-pyrone analogue

Furthermore, in order to be exploitable in biomedical applications and especially in photopharmacology a chromophore should present significant absorption in the biological optical active window, *i.e.* cover the 650 to 1350 nm range in the NIR region. As previously

said photoswitching of CC is instead induced by absorption in the UVA region, hence results inapplicable in a biological environment, due to the limited penetration and the possible toxicity of the incident light. One way to circumvent such a limitation resides in exploiting non-linear and in particular two-photon absorption (TPA) properties. Indeed, in this case the simultaneous absorption of two photons having a wavelength of about 740 nm, would be sufficient to populate the isomerizing excited state. Furthermore, TPA probability has a quadratic dependence to the light-source intensity, hence it decays more rapidly when moving away from the incident laser focal point, allowing for a better control of the spatial selectivity that is extremely important in biomedical application, such as photodynamic therapy. While we have shown that natural CC has a relatively high TPA cross-section compared to analogous organic compound, the calculated value of 14 GM is still too low for its veritable exploitation.[6] For all these reasons, we designed herein an analogue of cyclocurcumin with improved non-linear absorption properties and especially with significantly increased TPA cross-section.

We thus propose a 2,6-disubstituted-γ-pyrone analogue (Scheme 1) with an additional ethylene bond compared to the 2,3-dihydro-γ-pyrone core of CC to i) increase the planarity of the structure and to ii) introduce a second donor-acceptor group (aryl-ketone) increasing molecular symmetry. Indeed, planar and quadrupolar structures D-π-A- π -D, such as the one of pyrone, are expected to be more efficient in TPA than their dipolar analogues D-π-A, such as cyclocurcumin.[8]

Results and discussion

1. Equilibrium geometry

TPA cross-section efficiency in organic compounds can be easily related to their molecular structures. TPA efficiency is founded on a rather complex theory, developed by Maria Göppert-Mayer in 1931, and based on the presence of intermediate fictive states allowing to overcome the formally quantum-physically prohibited simultaneous absorption of two-photons. However, practical rules of the thumb relating TPA efficiency and the specific molecular architecture exist and can be used. In particular, it can be shown that planar and centrosymmetric arrangements are extremely beneficial to increase TPA cross-section. Analogously, the presence of charge-transfer excited states can also be pointed out for its most favorable influence. More specifically, quadrupolar molecules presenting an alternance of donor (D) and acceptor (A) units linked by conjugated bridges (π), *i.e.* D-π-A-π-D structures are most favorable molecular scaffolds to achieve high and exploitable cross-section and are more

efficient than their dipolar analogues D-π-A, such as CC.[8] When examining the molecular formula and the equilibrium geometry of cyclocurcumin, the breaking of the planarity induced by the free rotation of the phenyl group in position 2 can be seen as a further reason of the simulated moderate cross-section for the natural occurring compound. To fix the planarity issue, a most promising possibility could be to introduce a double bond leading to a pyrone core. Indeed, the optimization of the geometry of the thermodynamically favored E-isomer of γ-pyrone, performed at density functional (DFT) level of theory, has shown the quasi-planarity of the organic core (Figure 1) as also quantified by the dihedral angle between the phenyl ring and the pyrone moiety that reaches the value of 160° in contrast to the almost perpendicular arrangement observed for natural CC.

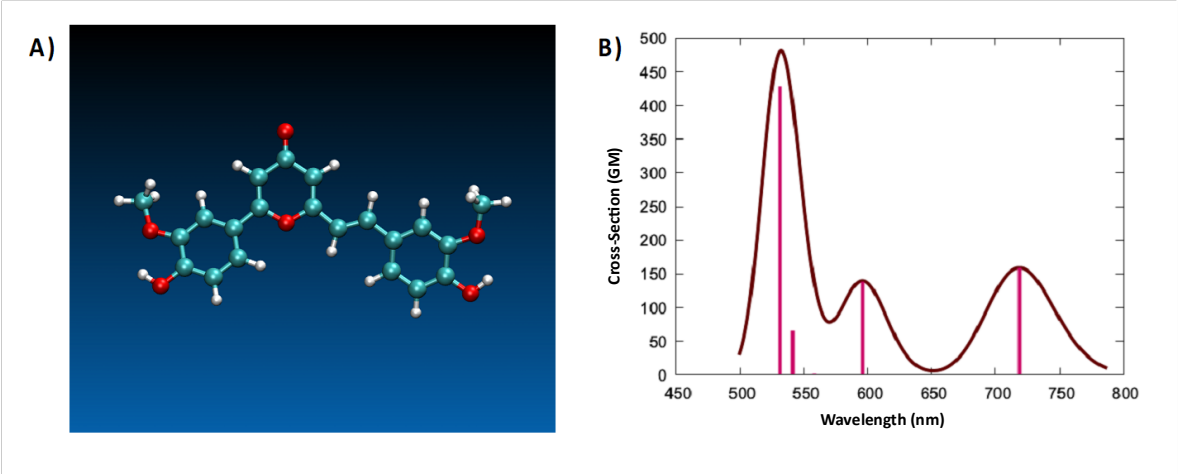

Figure 1. Equilibrium ground-state geometry simulated at DFT level (A) and TPA absorption spectrum (B) of our targeted 2,6-disubstituted-γ-pyrone **1** calculated at CAM-B3LYP level of theory. Note that the absorption spectrum has been obtained by convoluting the vertical transitions, represented as vertical sticks, with gaussian functions of fixed width at half-length of 0.3 eV.

The influence of the oxidation on the linear optical properties of our targeted compound, as obtained by state-of-the-art molecular modeling, will be discussed in the following. Here, and to justify the forthcoming synthetic efforts, we only report simulated TPA spectrum in water that would be the most relevant solvent for biological applications. Note that, as detailed in Section 3.1, CAM-B3LYP functional is the one better reproducing the optical properties of our compound, and hence was retained for modeling TPA. As can be seen from Figure 1, the simulated TPA previews that the non-linear absorption to the S_1 (π-π*) state will take place in

the NIR, with a maximum at 719 nm. Notably, the corresponding band is well separated from the one leading to the S_2 (n-π*) absorption and most importantly is characterized by a cross-section of 159 GM. This value represents an order of magnitude increase in the TPA performance over the parent CC, which peaked at only 14 GM in the NIR range.[6] This could be also assigned to the enhancement of planarity of the scaffold that leads to a quadrupolar arrangement of D-π-A-π-D type. Remarkably, absorption to the S_2 state also led to a band whose tails would partially cover the biological active window, peaking at around 600 nm and having cross-section of 139 GM. Absorption to higher excited states leads to band appearing in the visible part of the spectrum, and hence being less exploitable despite their high cross section.

Globally, the results of molecular modeling are consistent in previewing a considerable increase of the optical properties of the target biomimetic analogous, thus justifying the efforts in synthetic methodology that have been undertaken and that are presented in the following section.

2. Synthesis of 2,6-disubstituted-γ-pyrone analogue of cyclocurcumin

The retrosynthetic pathway proposed herein for the synthesis of targeted 2,6-disubstituted-γ-pyrone analogue of cyclocurcumin is given in Scheme 2. This consists in the aldolization/crotonization reaction of an alkylated vanillin and the methyl group of γ-pyrone **1** and leading to a photoisomerizable carbon-carbon double bond.

Our strategy was based on the formation of the γ-pyrone ring, the di-dehydrogenated equivalent of the 2,4-dihydro-γ-pyrone ring, present in cyclocurcumin. Various synthetic routes affording to symmetrically or asymmetrically in 2,6 positions were already described in the literature according to classical methods such as: (i) the cyclocondensation of the dienol of 1,3,5-tricarbonyl compounds under mild acidic catalysis (*i.e.* Brønsted acids such as triflic acid or *p*-toluenesulfonic acid),[9,10] (ii) the cyclization of diynone,[11,12,13] or *via* an original pathway using an isoxazole intermediate.[14] Herein, we chose to implement the strategies involving either a diynone intermediate, as the most explored and documented pathway to form a γ-pyrone ring, and the one involving an oxazole intermediate *a priori* faster and offering good yields. Thus, three synthetic ways were evaluated for the formation of the central pyrone moiety, namely (i) with nitro and terminal alkyne fragments **4** and **5a** (pathway 1, Scheme 2), (ii) alkyne **5a** and

butynal **6** (pathway 2, Scheme 2) or (iii) bromoguaiacol **7**, propargyl alcohol **8** and 1-propynylmagnesium bromide **9** (pathway 3, Scheme 2).

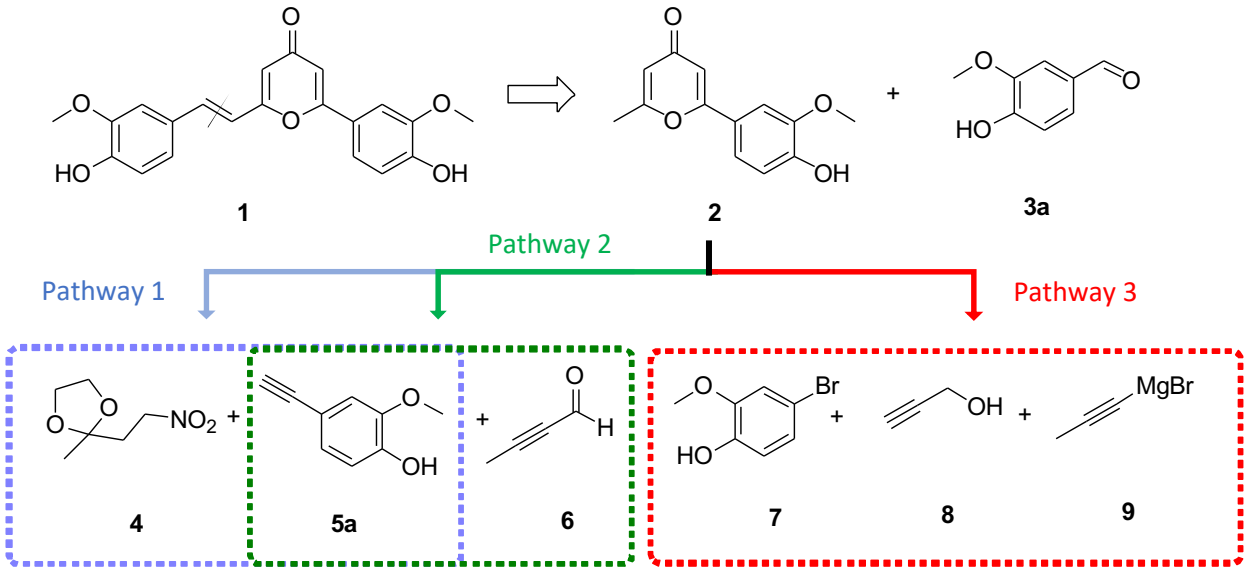

Scheme 2. Retrosynthetic pathways for the formation of dissymmetric γ-pyrone **1**

In the first pathway, the synthesis of **2** was envisaged through the synthesis of isoxazole intermediate **11**, which is previously generated from the two building blocks **4** and **5a** (Scheme 2, Pathway 1). This procedure is similar to the one previously reported by Li *et al.* and it is based on the 1,3-dipolar cycloaddition reaction between the acetylene **5a** and the nitrile oxide, generated *in situ* from fragment **4**.[14] According to the authors, the presence of the 2-oxoalkyl chain in position 3 of isoxazole should allow, after reduction by $Mo(CO)_6$ to an enamino ketone intermediate, which is cyclized under acidic conditions into the corresponding γ-pyrone **2**.

The general reaction scheme corresponding to the first retrosynthetic pathway is given in Schemes 3 and 4. Compounds **5a-c** (Scheme 3) could have been obtained one pot by transforming the aldehyde group of vanillin derivatives (**3a-c**) into a terminal alkyne as proposed by Doddi and coll.[15] This implies the use of modified Ramirez olefination[16,17] (CBr_4 and triisopropyl phospite $P(O^iPr)_3$ to avoid the elimination of triphenylphosphine oxides) followed by modified Corey-Fuchs reaction using the 1,8-diazabicyclo[5.4.0]undec-7-ene (DBU) and NaOH as base. Unfortunately, terminal alkynes **5a-c** could not be obtained according to this method. Thus, the synthesis was done in two-steps involving i) a Ramirez olefination of aldehyde to give 1,1'-dibromoalkenes **10a-c** in good yields then ii) Corey-Fuchs reaction (Scheme 3).[18,19] For this latest way, the reaction performed with DBU only led to very

low yields (< 10%).[20] Finally, the classical Corey-Fuchs reaction carried out with *n*-BuLi as base at -78°C gave the desired terminal alkynes **5a-c** with an excellent yield (Scheme 3).

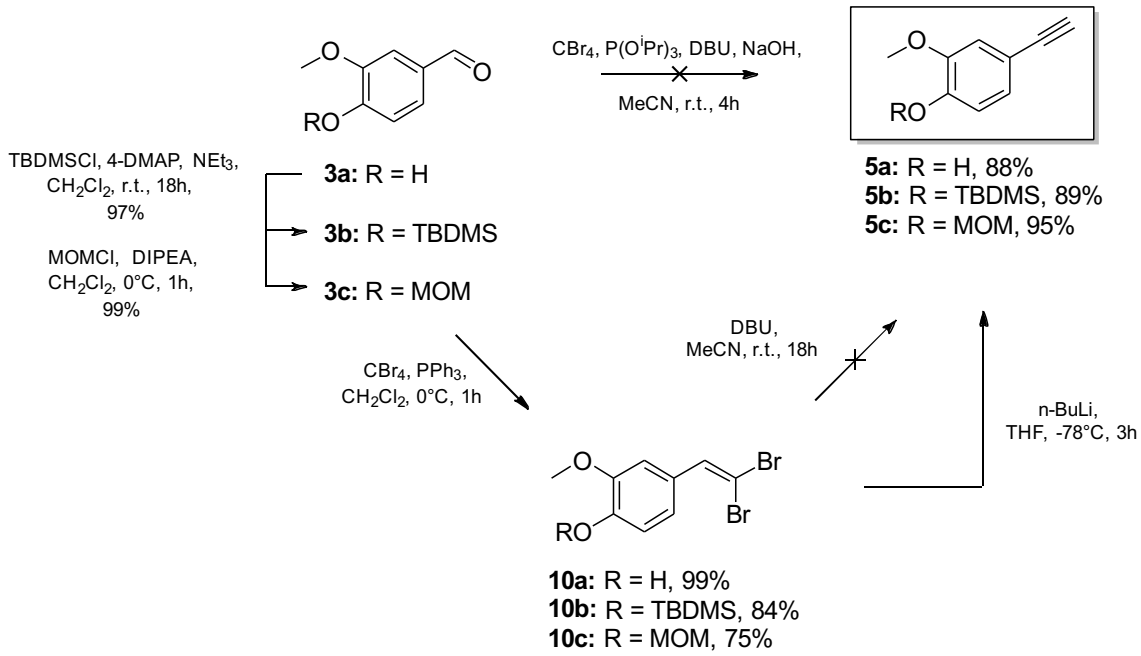

Scheme 3. Synthetic pathway to obtain terminal alkyne **5**.

In parallel, the synthon **4** was prepared, according to the literature, from methyl vinyl ketone and sodium nitrite in acidic conditions followed by carbonyl protection as dioxolane.[21,22] However, in our experiments, the two reaction steps afforded to yields lower than 30% as well as to the formation of the 1,4-adduct of the acetate on the conjugated carbonyl as main product. Then, the conversion of the **4** into the corresponding nitrile oxide precursor was tested *in situ* under Mukaiyama's dehydration conditions using phenyl isocyanate.[23] Unfortunately, the expected heterocyclic compounds **11a-c** could not be isolated, probably due to the instability of the nitro derivative **4** or the non-formation *in situ* of the nitrile oxide intermediate (Scheme 4). Therefore, this strategy was not further explored.

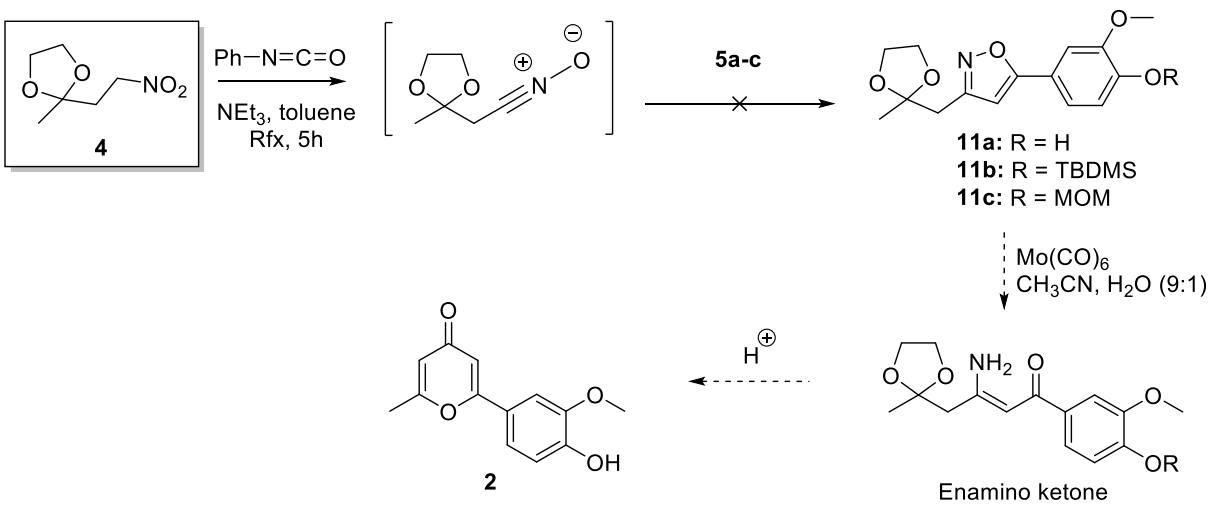

Scheme 4. First strategy considered to obtain the 2-aryl-γ-pyrone **2**

The second pathway envisaged to form γ-pyrone **2** was based on the internal cyclization of a diynone (Scheme 2, Pathway 2). In this second strategy the targeted intermediate was diynol **15**, which could be potentially synthesized from aldehyde **6** and the alkyne **5c** (Scheme 5), then oxidized in ketone and cyclized into **2**.

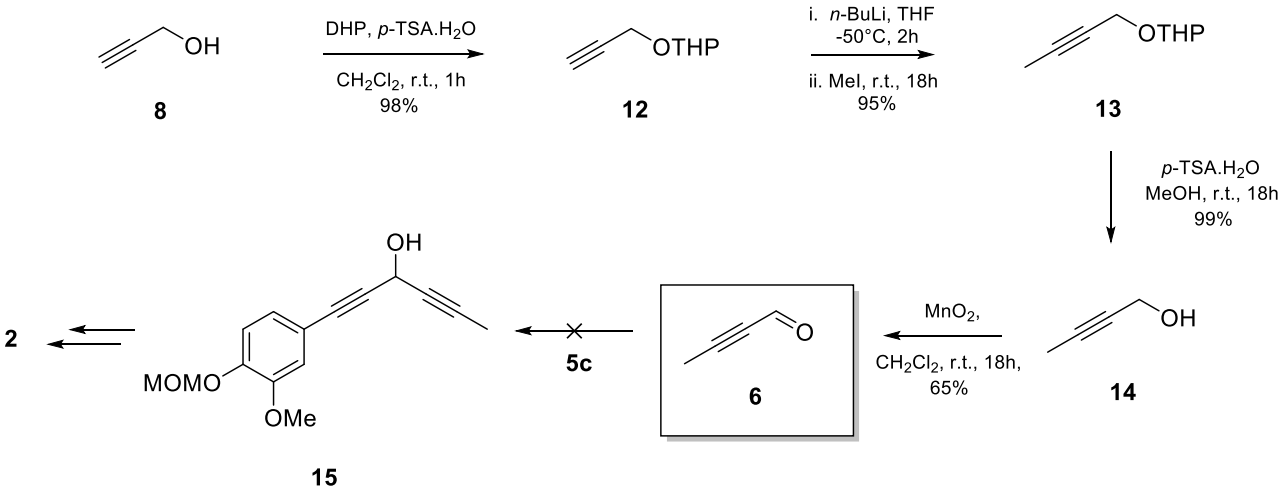

Scheme 5. Bottom-up approach to obtain the 2-aryl-γ-pyrone **2**.

In this bottom-up approach, the commercial propargyl alcohol (**8**) was easily protected as tetrahydropyranyl ether, compound **12,** with dihydropyrane (DHP) in CH_2Cl_2 and acidic media.[24,25] The terminal alkyne was then alkylated with methyl iodide and *n*-BuLi (Scheme 5,

compound **13**), and deprotected in the presence of *p*-TSA to give the expected 2-butynyl alcohol **14**.[26] The last was oxidized with an excess of MnO_2 to afford the corresponding 2-butynyl aldehyde **6**.[27] This aldehyde should have been coupled with terminal alkyne fragment protected terminal alkyne **5c** to give the diynol derivative **15**.[28,29] Unfortunately, in addition to partial polymerization (described as inevitable in the literature), the aldehyde **6** got oxidized into the corresponding carboxylic acid, and thus despite our various precautions (low temperature, dry and free oxygen conditions).[30] Thus, this strategy was not suitable for further developments.

Finally, the diynol **15** was synthesized from guaiacol (**16**) according to the third retrosynthetic pathway (Scheme 2) *via* a top-down approach. After a regioselective bromination with NBS (Scheme 6, compound **7**) and protection of phenolic function, the MOM protected bromoguaiacol was obtained with an overall yield of 90% (Scheme 6, compound **17**).[31,32,33] Then, a Sonogashira coupling using propargyl alcohol (**8**) in the presence of palladium complex catalyst as well as copper co-catalyst led to butynyl alcohol derivative **18** in good yield.[34] The oxidation with an excess of manganese dioxide gave aldehyde **19** which did not exhibit the instability of **6**.[27,35] The ynal **19** could undergo the addition of 1-propynylmagnesium bromide (**9**) to give the expected aryl-hexa-1,4-diyn-3-ol **15** with a yield of 89%.[11] The last step before the cyclization in γ-pyrone was the oxidation of **15** in corresponding ketone **20** using MnO_2.[11,36] Thus, according to this synthetic way the γ-pyrone's precursor **20** was obtained with an overall yield of 66%. Then, the cyclization of diynone **20** was performed *via* acid-mediated reaction (with triflic acid) in the presence of water, as previously described.[37] The target 2-aryl-γ-pyrone **2** was obtained with a good yield (52% in 7 steps) and was fully characterized by NMR, mass spectrometry and elemental analysis.

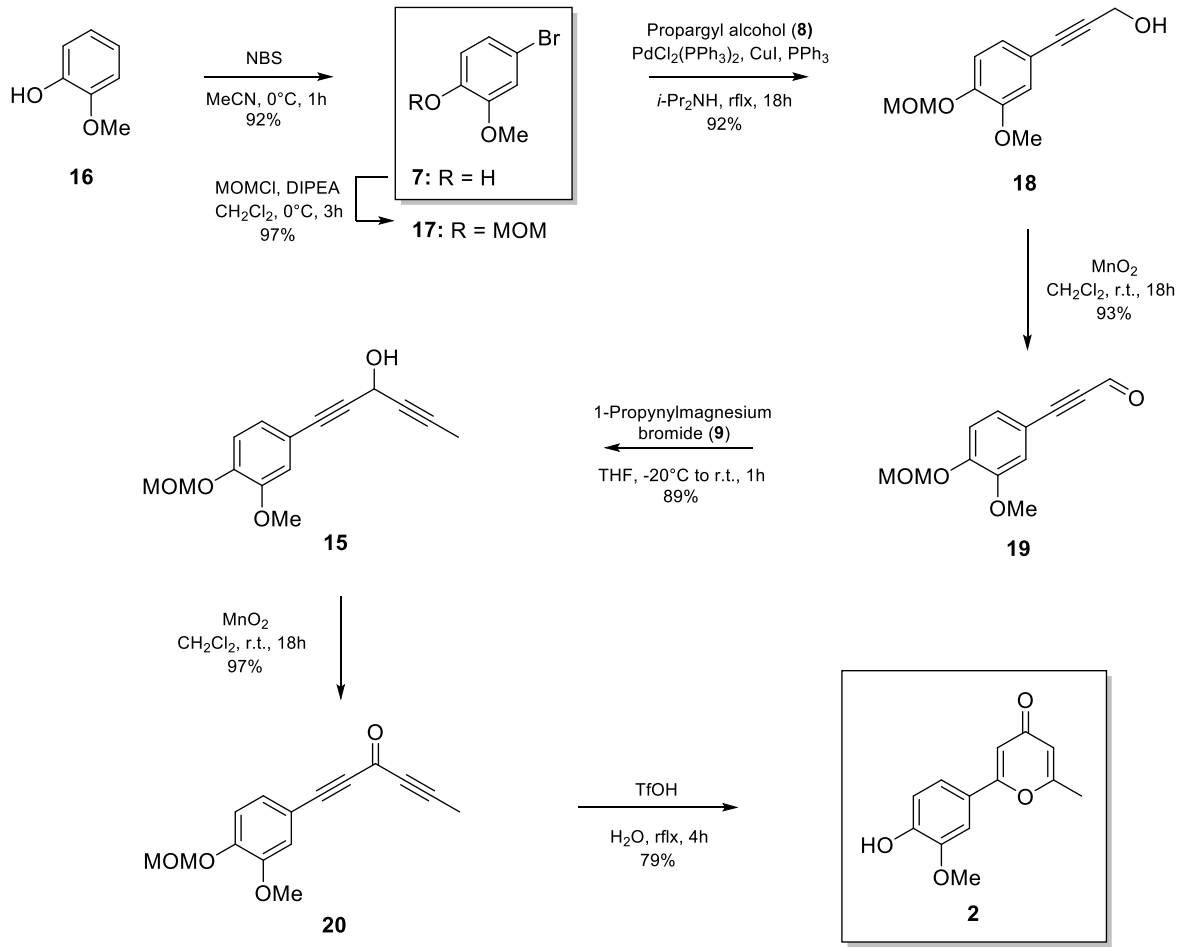

Scheme 6. Top-down approach leading to γ-pyrone core **2**.

To optimize the conditions of the aldolization/crotonization reaction between compounds **21** (MOM-protected γ-pyrone core) and **3c**, various parameters have been investigated, *i.e.* the nature and quantity of base, reaction time and temperature (Scheme 7 and Table 1).[38,39]

Table 1. Influence of the base, time, and temperature on the reaction yield and stereoselectivity between compounds **21** and **3c**.

Entry	Base	Time (h)	T (°C)	Yield (%)	*E/Z* molar ratio
1	NaOMe (1.2 eq)	18	25	Traces	n.d.
2	KOH (1.2 eq)	18	25	**21** degradation	n.d.
3	NaOEt (1.2 eq)	18	25	20	1/1
4	NaOEt (1.2 eq)	48	40	38	95/5

On one side, only traces of the expected alkene were obtained with solid sodium methanolate or potassium hydroxide, the latest even inducing the degradation of the pyrone cycle. On the

other side, the expected alkene was formed in moderate yield with freshly prepared sodium ethanolate. However, when the reaction was carried out at 25°C for 18 h, the product was isolated with only 20% yield and showed no stereoselectivity. An increase of the temperature to 40°C and reaction time to 48h was necessary to improve the conversion and to isolate after chromatography the product with 38% yield. In those conditions, an enhancement of stereoselectivity was observed, isomer *E* being the major stereoisomer.

The optimized conditions (Table 1, line 4) were then used to couple the protected aryl-γ-pyrone **21** (Scheme 7) with MOM-protected vanillin **3c**. The desired compound **22** was obtained with 38% yield. A final acidic deprotection of aryl-γ-pyrone moieties afforded quasi-quantitatively the target derivative **1,** analogue of cyclocurcumin.[40] This newly reported compound was fully characterized by NMR and HRMS which confirmed the molecular structure.

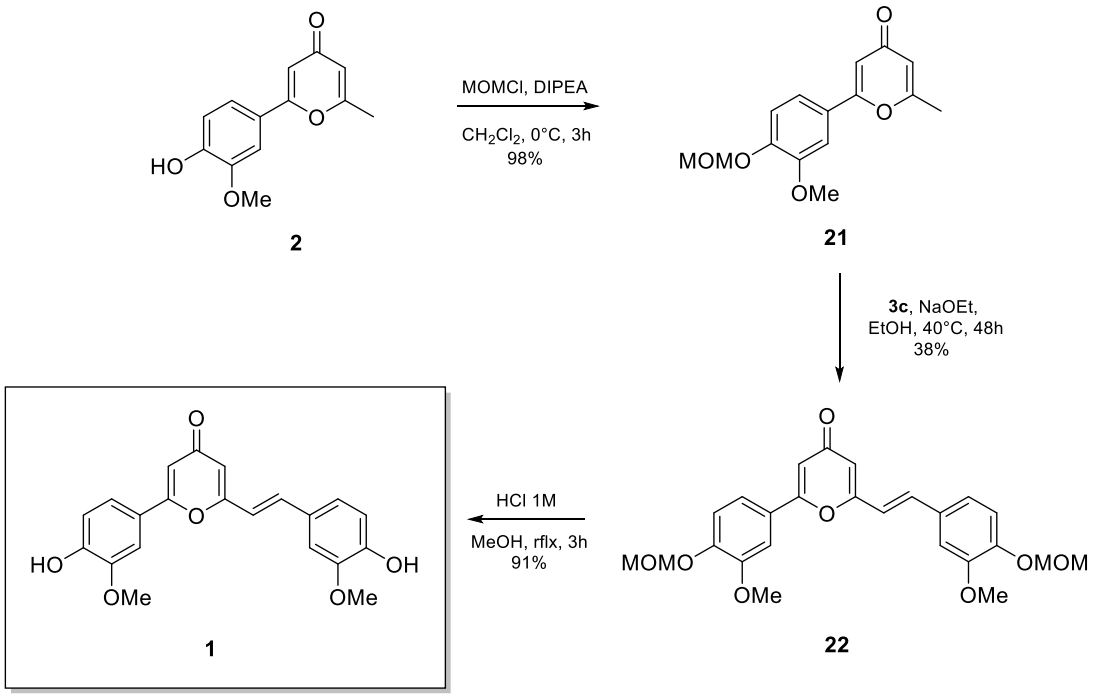

Scheme 7. Synthetic pathway leading to **1**, 2,6-disubstituted-γ-pyrone analogue of cyclocurcumin.

3. Photophysical properties of 2,6-disubstituted-γ-pyrone analogue of cyclocurcumin, 1

3.1. Simulated absorption and emission spectra.

One-photon absorption spectrum was computed for comparison with experiment. To that purpose, different DFT functionals and basis sets were benchmarked to characterize the excitation of the molecule, see in the ESI for more details.

CAM-B3LYP functional gave the best representation of the excited state manifold as compared to the other functional. This agreement holds despite a considerable shift in the absolute value of the absorption wavelengths that is common for range-separate functionals. It can be related to an improved representation of charge-transfer states compared to hybrid functionals that avoids the presence of significant intruder states, whose excitation energy would have been artificially lowered. In Figure 2, the calculated absorption spectrum is shown taking into account the vibrational and dynamic effects modeled *via* a Wigner distribution sampling around the stationary minimum. Also, the emission spectrum was calculated sampling the most stable minimum in the excited state in the gas phase. In the case of the absorption spectrum *in vacuo* we observe an absorption maximum at around 310 nm, while the emission spectrum is considerably stoked-shifted peaking at 375 nm. Note also the important asymmetry of the absorption band due to the vibronic coupling and the large and rather shoulderless emission band. Both absorption and emission spectra match reasonably with the experimental ones, reported in the next section.

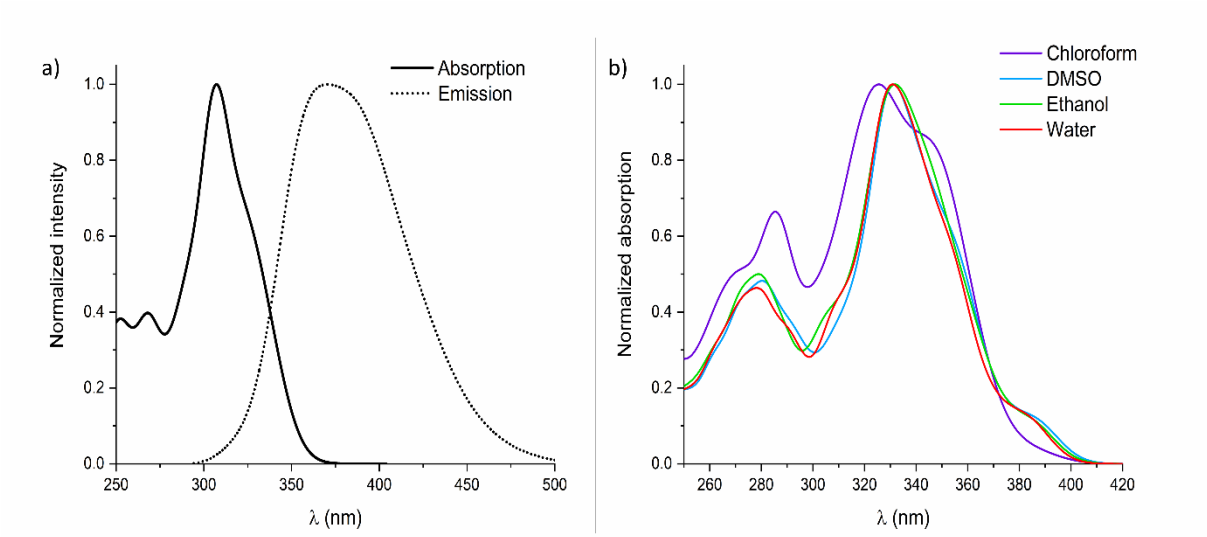

Figure 2. Absorption and emission spectra in the gas phase of 2,6-disubstituted-γ-pyrone analogue **1** at the CAM-B3LYP level (left). Absorption spectra in different solvents using PCM (right).

In conjunction with the gas phase exploration of the absorption and emissive properties, solvatochromism was investigated including the solvent effects implicitly via a dielectric medium in the polarizable continuum model (PCM) approach (Figure 2 right). A slight red shift of the absorption maximum was observed when increasing the polarity of the solvent. Most

remarkably, the spectrum in chloroform presents a noticeable shoulder at a wavelength higher than λ_{max}. The appearance of this feature might be due to a complex coupling between the electronic and nuclear degrees of freedom and most notably to the mixing of the lowest laying (n-π*) and (π-π*) states that is strongly dependent on the specific sampled geometry.

Moreover, the isomerization process was characterized by molecular modeling in a related publication.[41] It is shown that it occurs through the participation of the n-π* and the π-π* excited states. Notably, the process is more efficient than the one for natural CC, due to the lower energy barriers found along the isomerization coordinates of both excited states potential energy surfaces. The more efficient isomerization can also explain the lower fluorescence quantum yield due to the triggering of a reactive dissociative channel.

3.2. Experimental absorption and emission spectra.

The photochromic properties of the 2,6-disubstituted-γ-pyrone analogue of cyclocurcumin, **1**, were investigated in aprotic and protic solvents with various polarities (*i.e.* $CHCl_3$, MeCN, DMSO, EtOH and H_2O). The steady-state absorption spectra of the pyrone at the ground state are shown in Figure 3 and correspond mainly to the *E*-isomer as determined from NMR (Figure 5) (*E/Z* ratio of 100:0 in DMSO and 92:8 in EtOH). All spectra exhibit three broad absorption peaks, centered on ~ 288, 327 and 374 nm in ethanol. The highest and the lowest energy absorption band were assigned to be mainly due to the π–π* transition of the phenyl-pyrone moiety (D_1-π-A) and the styryl-pyrone moiety (A-π-D_2), respectively (Figure 3), while the intermediate energy absorption band was assigned to the n–π* transition. The values related to the styryl-pyrone moiety are similar to the ones reported for cyclocurcumin, which exhibit in ethanol a main absorption peak at ~370 nm and a shoulder at ~330 nm.[3] This is consistent with the fact that the additional double bond in the pyran cycle is not inducing any extension of π-conjugation on the styryl-pyrone moiety (A-π-D_2), but rather an extension of planarity from one extreme to the other of the molecule (Figure 1).

An overall positive solvatochromism is observed which corresponds to a bathochromic shift (or red shift) with increasing solvent polarity. This could be due to a more important stabilization of the bright state (π–π*) due to the higher dipolar moment of this excited state. The molar extinction coefficients (Table 2) at the respective maxima band are also depending on the

solvent, the highest value being obtained in MeCN (31654 M^{-1} cm^{-1}) and the lowest in H_2O (14632 M^{-1} cm^{-1}).

The fluorescence spectra of 2,6-disubstituted-γ-pyrone analogue of cyclocurcumin were obtained upon excitation at the maxima band (358 nm in chloroform, 354 nm in acetonitrile, 367 nm in DMSO, 371 nm in ethanol and 371 nm in water) and are given in Figure 3. Identical fluorescence spectra were obtained upon excitation at 320 nm in chloroform and acetonitrile, and 330 nm in DMSO, ethanol and water showing that the emission spectra is not depending on the excitation wavelength (Figure SI3). Whatever the solvent, a broad fluorescence spectrum is observed which maximum is Stokes shifted and is increasing with increasing solvent polarity. This indicates that the excited-state dipole moment of the pyrone is significantly larger than that of its ground state. Whatever the solvent, the quantum yields of fluorescence (ϕ) are low and do not exceed 2% (see Table 2). The lowest and the highest ϕ of 2,6-disubstituted-γ-pyrone were of 2% in DMSO and less than 1% in water, respectively. Those values are much lower than the one of cyclocurcumin which has a fluorescence quantum yield of 9% in chloroform (*vs* 1.5% for the pyrone analogue) and of 3% in acetonitrile (*vs* 1.3% for the pyrone analogue).[3]

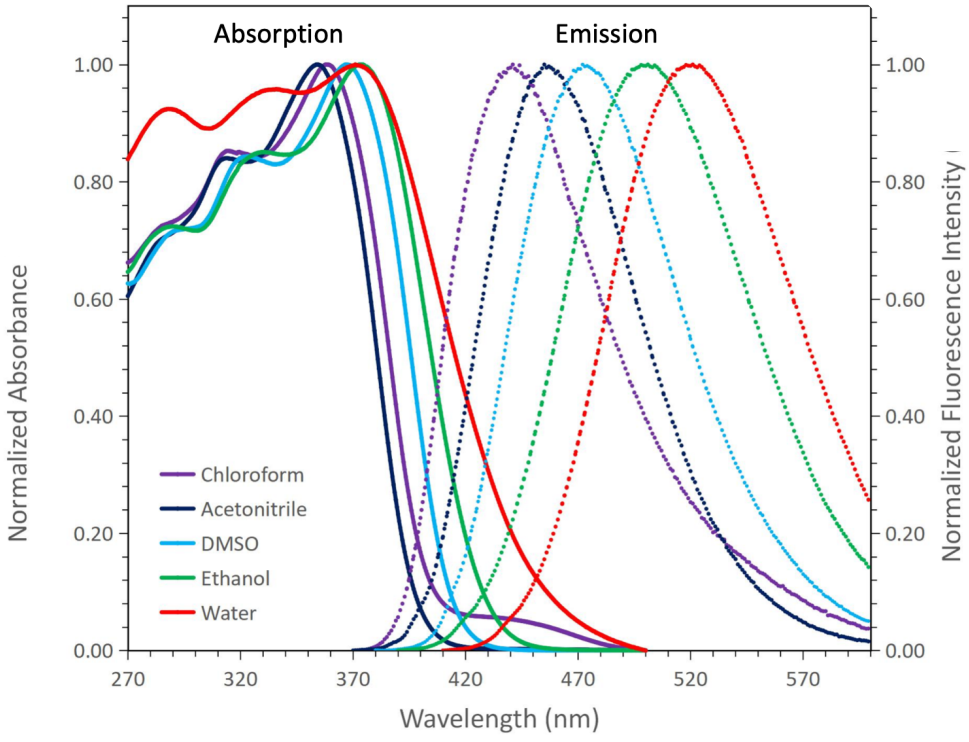

Figure 3. Normalized absorption (left) and emission (right) spectra of 2,6-disubstituted-γ-pyrone **1** upon excitation at λ_{max} in various solvents (at 358 nm in chloroform, 354 nm in acetonitrile, 367 nm in DMSO, 371 nm in ethanol and 371 nm in water).

Table 2. Optical properties of 2,6-disubstituted-γ-pyrone **1** and kinetics of the photoisomerization process.

	$CHCl_3$	CH_3CN	DMSO	EtOH	H_2O
λ_{abs} (nm)	358	354	367	374	371
ε_E (M^{-1} cm^{-1})	27000	31654	27927	27220	14632
λ_{em} (nm)	441	455	472	501	516
ϕ_F (%)	1.5	1.3	2.0	1.8	<1
E/Z* (GS)	n.d.	n.d.	100/0	92/8	n.d.
E/Z* (PSS)	n.d.	n.d.	47/53	25/75	n.d.
E*→*Z at 25°C, 375 nm**					
$k_{E\to Z}^{375}\cdot 10^3$ (s^{-1})	30	18	12	16	n.d.
$t_{1/2}^{375}$ (s)	23	39	58	43	n.d.
Z*→*E at 25°C, 300 nm**					
$k_{Z\to E}^{300}\times 10^3$ (s^{-1})	127	124	182	145	n.d.
$t_{1/2}^{300}$ (s)	5.5	5.6	3.8	4.8	n.d.
Z*→*E non-radiative (nr)**					
$k_{Z\to E}^{nr}\times 10^6$ (s^{-1}) at 25°C**	1.6	<1	<1	4.4	n.d.
$t_{1/2}^{nr}$ (h) at 25°C	120	>168	>168	44	n.d.
$k_{Z\to E}^{nr}\times 10^6$ (s^{-1}) at 40°C**	38.9	2.7	14.7	5.3	n.d.
$t_{1/2}^{nr}$ (h) at 40°C	5.0	71	13	36	n.d.

* as determined from NMR measurements.
** as determined from UV-VIS measurements.

The decrease in the fluorescence of 2,6-disubstituted-γ-pyrone **1** compared with cyclocurcumin could be attributed to the enhancement of nonradiative decay processes such as the excited-state isomerization of the styryl double bond. Moreover, this nonradiative deactivation process should be favored by the decrease of internal conversion of pyrone, more rigid and more planar than cyclocurcumin that can adopt several rotamers conformations. To further investigate this hypothesis, we characterize the photoisomerization process (Scheme 8) through combined steady-state absorption and NMR experiments.

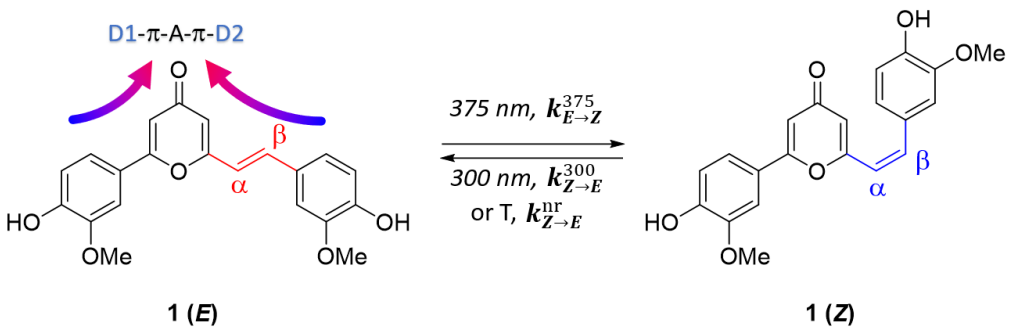

1 (*E*) **1 (*Z*)**

Scheme 8. Reversible *E*/*Z* photoisomerization scheme of the quadrupolar compound **1** showing direct isomerization upon irradiation at 375 nm and reverse reaction taking place either by irradiation at 300 nm or thermally, in the dark

3.3. Characterization of the photoisomerization efficiency.

The isomerization of 2,6-disubstituted-γ-pyrone is a reversible process in which (i) the direct isomerization consists in the photo-induced transformation of *E* into *Z*-isomer upon irradiation at a wavelength close to the λ_{max} of the *E*-isomer. The back-switch represents the reverse reaction that takes place either by irradiation at 300 nm or thermally, in the dark (Scheme 8). This process can be followed either by monitoring the time-evolution of the UV/Vis absorption spectrum and in particular of the intensity of the signature 370 and 300 nm bands (Figure 4), or the modification in the chemical shifts on the ^{1}H NMR spectra (Figure 5).

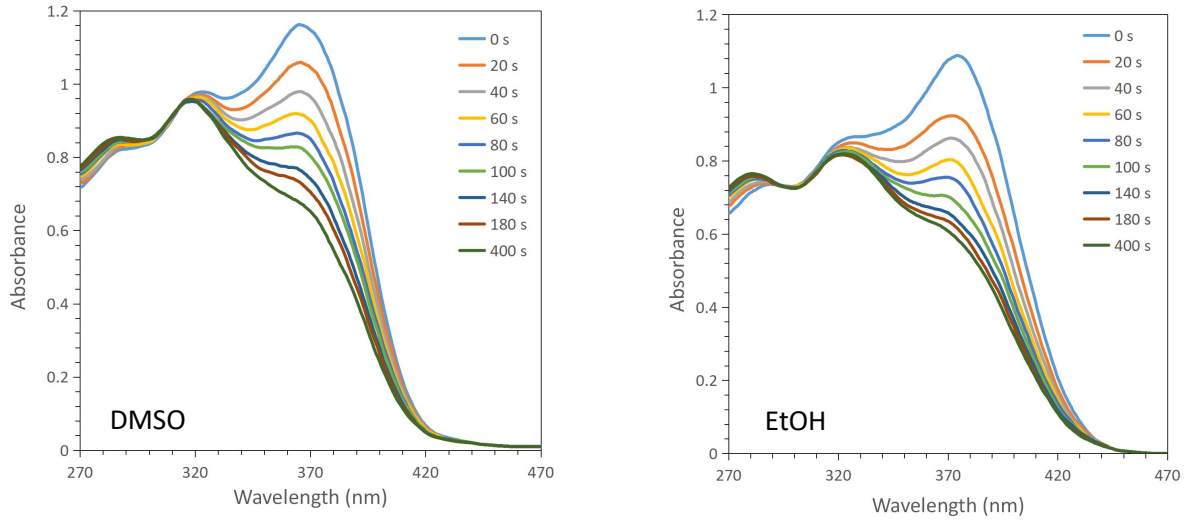

Figure 4. Spectral evolution the *E*→*Z* photoisomerization from the ground state to the photostationnary state, upon irradiation at 375 nm in DMSO (left) and in ethanol (right)

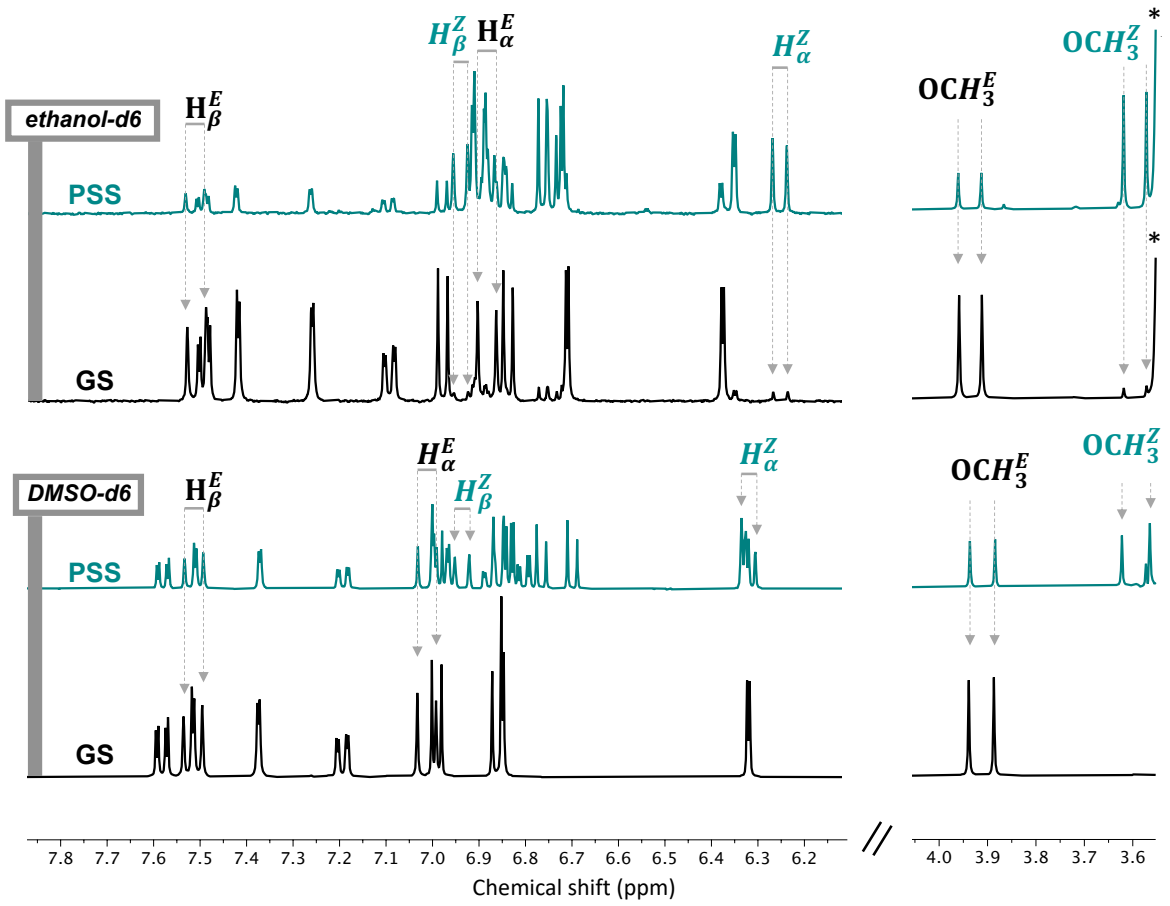

Figure 5. Representatative ^{1}H NMR spectra of the 2,6-disubstituted-γ-pyrone **1** in ethanol-*d6* and DMSO-*d6* at both ground state (black line) and photostationary state (cyan line).

At first, NMR experiments were performed to characterize both the ground state (GS) and the photostationary state (PSS). Full NMR spectra and peak positions of the 2,6-disubstituted-γ-pyrone 1 are provided in Supporting Information. While *E*-form is the thermodynamically favored isomer, the interconversion into *Z* can be induced upon irradiation at a wavelength close to the maximum absorption band, of about 370 nm. Figure 5 shows the most important changes in the ^{1}H NMR spectrum observed between the GS and the PSS, in ethanol-*d6* and DMSO-*d6*. For instance, in DMSO, the protons of the *E*-form of styryl moiety were assigned at 7.52 (H_{β}^{E}) and 7.01 (H_{α}^{E}) and the one of the *Z*-form at 6.94 (H_{β}^{Z}) and 6.32 ppm (H_{α}^{Z}). Those protons can be easily identified since the vicinal coupling constants are always larger for *E* (J_{HH} = 12-18 Hz, herein: 16.1 Hz) than for *Z*-isomers (J_{HH} = 0-12 Hz, herein: 12.1 Hz). As a general trend, the intensity of the protons of the *E* styryl moiety is decreasing upon excitation at 375 nm. However, they appear within a multiplet and therefore the accurate quantification of the *E/Z* ratio, via the peak integrals is rather cumbersome. Hence, we instead quantified the protons

belonging to the two -OCH_3 groups appearing at 3.94 and 3.89 for *E* isomer and at 3.62 and 3.56 for *Z*-isomer that are perfectly resolved and not overlapping (Figure 5). As indicated in Table 2, upon irradiation at λ_{max}, the *E/Z* ratio changed from 100/0 to 47/53 in DMSO and from 92/8 to 25/75 in ethanol. Interestingly, upon irradiation at 300 nm, the reverse, switch back process was not complete and yield *E/Z* ratio of 64/36 in both DMSO and ethanol. Moreover, the photoisomerization was perfectly reversible for at least 5 cycles under consecutive irradiation at 375 or 300 nm, respectively (Figure 6, left) and occurred within several minutes despite the moderate power of the LEDs used as illumination source (see Experimental section: kinetics and Figure 6 right, and SI4 and SI5).

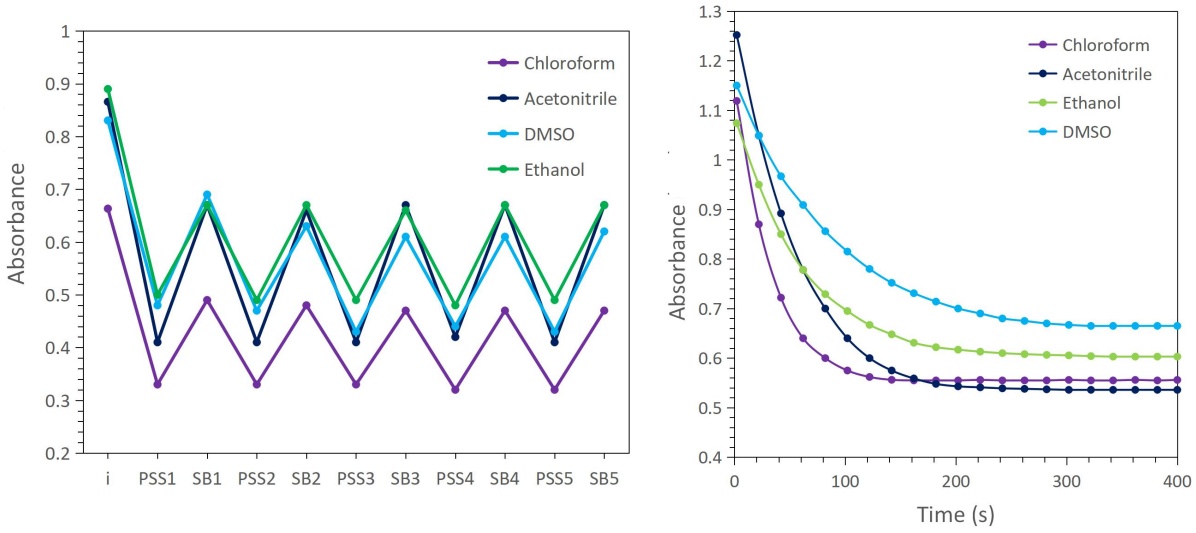

Figure 6. Absorption changes at λ_{max} during the succesive irradiation at two different wavelengths, 375 and 300 nm (left) and during the *E*→*Z* photoisomerization process at 375 nm as a function of time (right).

Figure 4 shows a typical evolution of the absorption band of 2,6-disubstituted-γ-pyrone upon irradiation at 375 nm in EtOH and DMSO. Additional UV spectra of the direct and reverse switch in chloroform and acetonitrile are given in SI. From the kinetic profiles of the direct and reverse switch (Figure 6 right), one can determine the kinetic parameters such as isomerization half-life times and rate constants (Table 2). It was observed that the rate constant of the direct *E* →*Z* switch decreases with increasing the polarity of the solvent, from 30×10^{-3} s^{-1} in chloroform to 16×10^{-3} s^{-1} in ethanol, except for DMSO, more viscous, for which $\boldsymbol{k}_{\boldsymbol{E\rightarrow Z}}^{\boldsymbol{375}}=12\times10^{-3}$ s^{-1}. On the contrary, the highest rate constant of the reverse reaction, under irradiation at 300 nm, was obtained in DMSO, $\boldsymbol{k}_{\boldsymbol{Z\rightarrow E}}^{\boldsymbol{300}}=182\times10^{-3}$ s^{-1}. On the other side, the thermal back-switch

was extremely slow $k_{Z\rightarrow E}^{nr}$<1×10^{-6} s^{-1} at 25°C and only slightly increases to $k_{Z\rightarrow E}^{nr}$=14.7×10^{-6} s^{-1} at 40°C (Figure SI6). This negligible thermal switch is of paramount importance for a high temporal control of the switch, only triggered by irradiation.

Conclusion

In summary, we designed and synthesized a 2,6-disubstituted-γ-pyrone analogue of cyclocurcumin, a natural photoswitch in the UV-Vis region, in order to improve its photophysical properties and more particularly to increase the cross-section value of two-photon absorption.[42] Indeed, this feature is compulsory for further *in vivo* applications for which irradiation in the NIR region is needed. To do so, three retrosynthetic pathways were explored. While the passage through an isoxazole intermediate could have been more straightforward and could provide the target final molecule in only 5 steps instead of 10, the corresponding yields were too low (<30 %). Therefore, the pathway involving the cyclization of a diynone was preferred. In this case, we showed that the choice of the starting substrate, guaiacol *vs* propargyl alcohol, is of paramount importance as is conditioning the formation of highly reactive and volatile intermediates such as 2-butynyl aldehyde, if propargyl alcohol is used. Thus, the diynone was build step-by-step, through a bottom-up approach from guaiacol, followed by its cyclization and by the formation of the carbon-carbon double bond *via* an aldolization/crotonization reaction on the residual methylene of the pre-formed pyrone ring. Finally, it was shown that the isomerization of the resulted analogue is a reversible process in which (i) the direct isomerization consists in the transformation of *E*-pyrone into *Z*-pyrone upon irradiation at 375 nm and (ii) the back-switch is the reverse reaction that takes place either by irradiation at 300 nm or thermally, in the dark. The 2,6-disubstituted-γ-pyrone analogue of cyclocurcumin showed excellent photoswitching properties, a low fatigue over at least 5 cycles and a better stability compared to cyclocurcumin. Due to the planar pyrone moiety of the quadrupolar D-π-A-π-D system, the value of two-photon cross-section (159 GM) was higher than the one of cyclocurcumin (14GM), as estimated from DFT calculations. Moreover, we have shown that, differently from CC, photoswitching happens with significant yields rather independently from the solvent polarity. Hence, we believe that our molecular design has tuned the competition between the different relaxation pathways favoring isomerization over fluorescence. All together our results indicate that our designed compound is of interest for

further applications as a molecular photoswitch activable via TPA excitation, and hence could be potentially used in biomedical field.

Experimental Section

General

All reactions were carried out under argon atmosphere. Toluene and THF were dried using a MBRAUN MB-SPS-800 solvent purification system. Other solvents and liquid reagents were purified and dried according to recommended procedures. Chemical reagents were purchased from Merck, Fisher Scientific or Sigma-Aldrich and were used as received. Analytical thin-layer chromatography (TLC) analyses were performed using standard procedures on silica gel 60 F254 plates (Merck). Compounds were visualized with UV light (254 nm) and alternatively, a potassium permanganate aqueous solution was used. Silica gel column chromatography was performed on a glass column filled with silica gel (63-200 μm) (Merck). Melting points (M.p.) were determined with a Tottoli apparatus and are uncorrected. Spectroscopic analyses and kinetic measurements were carried out on the PhotoNS Platform of the L2CM Laboratory, University of Lorraine. FTIR spectra were recorded on a Shimadzu IRAffinity-1 apparatus equipped with an ATR PIKE Technologies model GladiATR (cm^{-1}). NMR spectra were recorded at 300 K, unless stated otherwise, using a Bruker DRX400 spectrometer (400 MHz for ^{1}H and 100.6 MHz for ^{13}C). Chemical shifts are reported in ppm (δ) relative to deuterated solvent residual peaks. For complete assignment of ^{1}H and ^{13}C signals, two-dimensional ^{1}H, ^{1}H COSY and ^{1}H, ^{13}C correlation spectra were recorded. The following abbreviations are used to explain the observed multiplicities: s, singlet; d, doublet; dd, doublet of doublets; ddd, doublet of doublets of doublets; t, triplet; td, triplet of doublets; m, multiplet; bs, broad singlet. High resolutions mass spectra (HRMS) were recorded on a microTOFQ (Bruker) ESI/QqTOF spectrometer. The compounds **3b**, **3c**, **4**, **5b** and **10b** used in the first pathway were synthesized according to the methods reported in the references 43, 44, 21, 18 and 19 respectively. According to the second pathway, compounds **12**, **13** and **14** were obtained by following reference 26 and derivative **6** according to reference 27. Compounds **7** and **17**

used in third pathway were synthesized according to the methods described in reference 33 and 32, respectively.

Synthesis

4-(2,2-dibromovinyl)-2-methoxyphenol, 10a: To a stirred solution of vanillin **3a** (2.05 g, 13.44 mmol) and CBr_4 (8.95 g, 26.98 mmol, 2.0 eq.) in dry DCM (40 mL) at 0°C was added fractionally PPh_3 (14.21 g, 54.19 mmol, 4.0 eq.). The mixture was further stirred for 3h at 0°C (CCM, SiO_2, Cyclohexane/EtOAc, 85:15). The reaction mixture was quenched with water (30 mL) and the organic phase was separated. The aqueous phase was further extracted with DCM (3x30 mL). The combined organic phases were washed with water (3x30 mL) and brine (3x30 mL), then dried over Na_2SO_4, filtered and evaporated under reduced pressure. Purification by chromatography (SiO_2, Cyclohexane/EtOAc, 85:15) afforded compound **10a** as a yellow oil (4.12 g, 99%). ***Rf***: 0.38 (Cyclohexane/EtOAc, 85:15); **^{1}H NMR** (400 MHz, $CDCl_3$): δ=7.39 (s, 1H; Ar-C*H*), 7.19 (d, $J_{H,H}$=1.8 Hz, 1H; Ar-*H*), 7.04 (dd, $J_{H,H}$=8.3, 1.9 Hz; Ar-*H*), 6.91 (d, $J_{H,H}$=8.2 Hz, 1H; Ar-*H*), 5.85 (s, 1H; O*H*), 3.89 (s, 3H; OCH_3); **^{13}C{^{1}H} NMR** (100 MHz, $CDCl_3$): δ=146.3, 146.2, 136.6, 127.5, 122.8, 114.4, 110.6, 87.2, 56.1. **ESI-MS** (HR) *m/z:* $[M+Na]^+$ calcd for $C_9H_8{}^{79}Br_2NaO_2$: 328,8783, found: 328.8784.

4-(2,2-dibromovinyl)-2-methoxy-1-(methoxymethoxy)benzene, **10c**: To a stirred solution of 3-methoxy-4-(methoxymethoxy)benzaldehyde **3c** (503 mg, 2.56 mmol) and CBr_4 (1.72 g, 5.19 mmol, 2.0 eq.) in dry DCM (50 mL) at 0°C was added PPh_3 (2.71 g, 10.33 mmol, 4.0 eq.) fractionally and the mixture was stirred 3h at 0°C (CCM, SiO_2, Cyclohexane/EtOAc 95:5). The reaction mixture was quenched with water (30 mL) and the organic phase was separated. The aqueous phase was further extracted with DCM (3x30 mL). The combined organic phase was washed with water (3x30 mL) and brine (3x30 mL) then dried over Na_2SO_4, filtered and evaporated under reduced pressure. Chromatography on silica gel with EtOAc (2%) in cyclohexane afforded the title compound **10c** as a yellow oil (675 mg, 75%). ***Rf***: 0.29 (Cyclohexane/EtOAc 95:5). **^{1}H NMR** (400 MHz, $CDCl_3$): δ=7.41 (s, 1H; Ar-C*H*), 7.19 (d, $J_{H,H}$=1.3 Hz, 1H; Ar-*H*), 7.06 (d, $J_{H,H}$=8.4 Hz, 1H; Ar-*H*), 7.04 (dd, $J_{H,H}$=8.4, 1.3 Hz, 1H; Ar-*H*), 5.24 (s, 2H; OCH_2O), 3.88 (s, 3H; OCH_3), 3.51 (s, 3H; OCH_3). **^{13}C{^{1}H} NMR** (100 MHz, $CDCl_3$): δ=149.4, 146.9, 136.5, 129.6, 122.0, 115.9, 111.8, 95.4, 88.1, 56.4, 56.1. **ESI-MS** (HR) *m/z:* $[M+H]^+$ calcd for $C_{11}H_{13}{}^{79}Br_2O_3$: 350.9226, found: 350.9236; *m/z:* $[M+Na]^+$ calcd for $C_{11}H_{12}{}^{79}Br_2NaO_3$: 372.9045, found: 372.9053.

4-ethynyl-2-methoxyphenol, 5a: To a stirred solution of 4-(2,2-dibromovinyl)-2-methoxyphenol **10a** (3.00 g, 9.73 mmol) in dry THF (100 mL) at -78°C was added *n*-BuLi (1.4 M in THF, 28 mL, 39.20 mmol, 4.0 eq.) dropwise and the mixture was stirred 3h at -78°C (CCM, SiO_2, Cyclohexane/EtOAc 85:15). The reaction mixture was quenched with NH_4Cl (70 mL) and the organic phase was separated. The aqueous phase was further extracted with DCM (3x50 mL). The combined organic phase was washed with water (3x50 mL) and brine (3x50 mL) then dried over Na_2SO_4, filtered, and evaporated under reduced pressure. Chromatography on silica gel with EtOAc (15%) in cyclohexane afforded the title compound **5a** as a brown oil (1.27 g, 88%). **^{1}H NMR** (400 MHz, $CDCl_3$): δ=7.06 (dd, $J_{H,H}$=8.2, 1.7 Hz, 1H; Ar-*H*), 6.98 (d, $J_{H,H}$=1.6 Hz, 1H; Ar-*H*), 6.86 (d, $J_{H,H}$=8.2 Hz, 1H; Ar-*H*), 5.83 (s, 1H; O*H*), 3.87 (s, 3H; OCH_3), 2.99 (s, 1H; C*H*). The NMR data are in agreement with the literature.[45]

4-ethynyl-2-methoxy-1-(methoxymethoxy)benzene, **5c**: To a stirred solution of 4-(2,2-dibromovinyl)-2-methoxy-1-(methoxymethoxy)benzene **10c** (150 mg, 0.43 mmol) in dry THF (30 mL) at -78°C was added *n*-BuLi (1.4 M in THF, 0.8 mL, 1.12 mmol, 2.6 eq.) dropwise and the mixture was stirred 3h at -78°C (CCM, SiO_2, Cyclohexane/EtOAc 9:1). The reaction mixture was quenched with NH_4Cl (20 mL) and the organic phase was separated. The aqueous phase was further extracted with DCM (3x20 mL). The combined organic phase was washed with water (3x20 mL) and brine (3x20 mL) then dried over Na_2SO_4, filtered, and evaporated under reduced pressure. Chromatography on silica gel with EtOAc (10%) in cyclohexane afforded the title compound **5c** as a yellow oil (79 mg, 95%). ***R**f*: 0.32 (Cyclohexane/EtOAc 9:1). **^{1}H NMR** (400 MHz, $CDCl_3$): δ=7.09-7.05 (m, 2H; Ar-*H*), 7.01 (m, 1H; Ar-*H*), 5.23 (s, 2H; OCH_2O), 3.87 (s, 3H; OCH_3), 3.50 (s, 3H; OCH_3), 3.01 (s, 1H; C*H*). **^{13}C{^{1}H} NMR** (100 MHz, $CDCl_3$): δ=149.5, 147.5, 125.6, 116.1, 116.0, 115.5, 95.5, 83.8, 76.1, 56.4, 56.1. **ESI-MS** (HR) *m/z:* $[M+H]^+$ calcd for $C_{11}H_{13}O_3$: 193.0859, found: 193.0841; *m/z:* $[M+Na]^+$ calcd for $C_{11}H_{12}NaO_3$: 215.0679, found: 215.0670.

3-(3-methoxy-4-(methoxymethoxy)phenyl)prop-2-yn-1-ol, 18: To a stirred solution of 4-bromo-2-methoxy-1-(methoxymethoxy)benzene **17** (3.80 g, 15.39 mmol) in diisopropylamine (^{i}Pr$_2$NH, 80 mL) was added $PdCl_2(PPh_3)_2$ (0,22g, 0.32 mmol, 0.02 eq.), CuI (0,12 g, 0.62 mmol, 0.04 eq.) and PPh_3 (0,16g, 0.62 mmol, 0.04 eq.). The solution was extensively degassed by argon bubbling. Propargyl alcohol (**8**) (1.20 mL, 20.32 mmol, 1.32 eq.) was added and the mixture was stirred overnight at 80°C with a heating mantle (CCM, SiO_2, Cyclohexane/EtOAc, 3:1). After cooling and filtration on a short pad of silica gel eluted with EtOAc, the resulting filtrate was washed with water (3x50 mL) and brine (3x50 mL), then dried over Na_2SO_4,

filtered, and purified by chromatography (SiO_2, Cyclohexane/EtOAc, 8:2 to 1:1) to afford the compound **18** as a brown oil (3.14 g, 92%). ***R_f***: 0.27 (Cyclohexane/EtOAc, 1:1). **IR** (ATR, cm^{-1}): ν: 3385 (OH), 2230. **^{1}H NMR** (400 MHz, $CDCl_3$): δ=7.08 (d, $J_{H,H}$=8.3 Hz, 1H; Ar-*H*), 7.00 (dd, $J_{H,H}$=8.3, 1.8 Hz, 1H; Ar-*H*), 6.97 (d, $J_{H,H}$=1.8 Hz, 1H; Ar-*H*), 5.23 (s, 2H; OC*H*$_2$O), 4.49 (d, $J_{H,H}$=4.8 Hz, 2H; C*H*$_2$), 3.87 (s, 3H; OC*H*$_3$), 3.51 (s, 3H; OC*H*$_3$), 2.27 (br s, 1H; O*H*). **^{13}C{^{1}H} NMR** (100 MHz, $CDCl_3$): δ=149.4, 147.1, 125.0, 116.5, 116.0, 115.0, 95.4, 86.3, 85.5, 56.4, 56.0, 51.6. **ESI-MS** (HR) *m/z:* $[M+H]^+$ calcd for $C_{12}H_{15}O_4$: 223.0965, found: 223.0974; *m/z:* $[M+Na]^+$ calcd for $C_{12}H_{14}NaO_4$: 245.0784, found: 245.0795.

3-(3-methoxy-4-(methoxymethoxy)phenyl)propiolaldehyde, 19: A suspension of MnO_2 (11.80 g, 0.136 mol, 10 eq.) in dry DCM (120 mL) was added to 3-(3-methoxy-4-(methoxymethoxy)phenyl)prop-2-yn-1-ol **18** (3.02 g, 13.61 mmol) and stirred overnight at room temperature (CCM, SiO_2, Cyclohexane/EtOAc, 3:1). Filtration on a short pad of silica gel eluted with DCM gave a filtrate which was concentrated and chromatographed (SiO_2, Cyclohexane/EtOAc, 75:25) to afford compound **19** as a brown oil (2.79 g, 93%). ***R_f***: 0.37 (Cyclohexane/EtOAc, 3:1). **IR** (ATR, cm^{-1}): 2176, 1647 (CH=O). **^{1}H NMR** (400 MHz, $CDCl_3$): δ=9.39 (s, 1H; C*H*O), 7.22 (dd, $J_{H,H}$=8.4, 1.9 Hz, 1H; Ar-*H*), 7.15 (d, $J_{H,H}$=8.4 Hz, 1H; Ar-*H*), 7.11 (d, $J_{H,H}$=1.8 Hz, 1H; Ar-*H*), 5.28 (s, 2H; OC*H*$_2$O), 3.89 (s, 3H; OC*H*$_3$), 3.51 (s, 3H; OC*H*$_3$). **^{13}C{^{1}H} NMR** (100 MHz, $CDCl_3$): δ=176.8, 149.8, 149.6, 127.7, 116.2, 115.8, 112.8, 96.3, 95.3, 88.5, 56.6, 56.2. **ESI-MS** (HR) *m/z:* $[M+H]^+$ calcd for $C_{12}H_{13}O_4$: 221.0808, found: 221.0802; *m/z:* $[M+Na]^+$ calcd for $C_{12}H_{12}NaO_4$: 243.0628, found: 243.0631.

1-(3-methoxy-4-(methoxymethoxy)phenyl)hexa-1,4-diyn-3-ol, 15: To a solution of 3-(3-methoxy-4-(methoxymethoxy)phenyl)propiolaldehyde **19** (0.33 g, 1.50 mmol) in anhydrous THF (5 mL) was added 1-propynylmagnesium bromide (**9**) (0.50M solution in THF, 4.50 mL, 2.25 mmol, 1.50 eq.) at -20°C and stirred for 0.5h. Stirring was maintained for another 1h at room temperature (CCM, SiO_2, Cyclohexane/EtOAc, 4:1). The reaction mixture was then quenched with saturated aqueous NH_4Cl (3 mL) and the organic phase was separated. The aqueous phase was further extracted with DCM (3x5 mL) and the combined organic phases were washed with water (3x5 mL) and brine (3x5 mL), then dried over Na_2SO_4 and filtered. The concentrated filtrate was purified by chromatography (SiO_2, Cyclohexane/EtOAc, 8:2 to 1:1) to afford the diynol **15** as a yellow oil (0.347 g, 89%). ***R_f***: 0.22 (Cyclohexane/EtOAc, 4:1). **IR** (ATR, cm^{-1}): 3354 (OH), 2181. **^{1}H NMR** (400 MHz, $CDCl_3$): δ=7.06 (d, $J_{H,H}$=8.3 Hz, 1H; Ar-*H*), 7.01 (dd, $J_{H,H}$=8.3, 1.8 Hz, 1H; Ar-*H*), 6.98 (d, $J_{H,H}$=1.7 Hz, 1H; Ar-*H*), 5.30 (br s, 1H; O*H*), 5.22 (s, 2H; OC*H*$_2$O), 3.85 (s, 3H; OC*H*$_3$), 3.49 (s, 3H; OC*H*$_3$), 2.52 (d, $J_{H,H}$=5.0 Hz, 1H;

C*H*), 1.88 (d, $J_{H,H}$=2.2 Hz, 3H; CH_3). **^{13}C{^{1}H} NMR** (100 MHz, $CDCl_3$): δ=149.4, 147.5, 125.3, 116.0, 115.9, 115.2, 95.5, 85.5, 84.1, 83.3, 81.6, 56.5, 56.1, 53.0, 3.9. **ESI-MS** (HR) *m/z:* $[M+H]^+$ calcd for $C_{15}H_{17}O_4$: 261.1121, found: 261.1136; *m/z:* $[M+Na]^+$ calcd for $C_{15}H_{16}NaO_4$: 283.0941, found: 283.1018.

1-(3-methoxy-4-(methoxymethoxy)phenyl)hexa-1,4-diyn-3-one, 20: MnO_2 (9.49 g, 0.109 mol, 20 eq.) was added into a solution of 1-(3-methoxy-4-(methoxymethoxy)-phenyl)-propiolaldehyde **15** (1.41 g, 5.43 mmol) in dry DCM (50 mL). The mixture was stirred overnight at room temperature (CCM, SiO_2, Cyclohexane/EtOAc, 4:1). The reaction mixture was then filtered on a short pad of silica gel eluted with DCM, the resulting filtrate was concentrated and purified by chromatography (SiO_2, Cyclohexane/EtOAc, 85:25) to give the diynone **20** as a brown oil (1.36 g, 97%). ***R$_f$***: 0.31 (Cyclohexane/EtOAc, 4:1). **IR** (KBr): 2181, 1616 (C=O). **^{1}H NMR** (400 MHz, $CDCl_3$): δ=7.23 (dd, $J_{H,H}$=8.4, 1.9 Hz, 1H; Ar-*H*), 7.14 (d, $J_{H,H}$=8.4 Hz, 1H; Ar-*H*), 7.12 (d, $J_{H,H}$=1.8 Hz, 1H; Ar-*H*), 5.28 (s, 2H; OCH_2O), 3.89 (s, 3H; OCH_3), 3.51 (s, 3H; OCH_3), 2.10 (s, 3H; CH_3). **^{13}C{^{1}H} NMR** (100 MHz, $CDCl_3$): δ=161.0, 149.7, 149.5, 127.8, 116.0, 115.7, 112.8, 95.3, 91.6, 91.4, 89.3, 81.6, 56.6, 56.2, 4.5. **ESI-MS** (HR) *m/z:* $[M+H]^+$ calcd for $C_{15}H_{15}O_4$: 259.0965, found: 259.0979; *m/z:* $[M+Na]^+$ calcd for $C_{15}H_{14}NaO_4$: 281.0784, found: 281.0807.

2-(4-hydroxy-3-methoxyphenyl)-6-methyl-4H-pyran-4-one, 2: TfOH (2.4 µL, 27.12 mmol, 1.0 eq.) was added dropwise to a solution of 1-(3-methoxy-4-(methoxymethoxy)phenyl)hexa-1,4-diyn-3-one **20** in deionized water (77 mL) and the mixture was stirred 4h at 100°C with a heating mantle (CCM, SiO_2, EtOAc/MeOH, 9:1). After cooling to room temperature, the reaction mixture was diluted with water (20 mL) and EtOAc (20 mL). The organic phase was separated, and the aqueous phase was further extracted with EtOAc (3x20 mL). The combined organic phases were washed with water (3x20 mL) and brine (3x20 mL), then dried over Na_2SO_4 and filtered. The filtrate was chromatographed (SiO_2, EtOAc/MeOH, 9:1) and afforded compound **2** as a white solid (4.95 g, 79%). ***R$_f$***: 0.34 (EtOAc/MeOH, 9:1). **M.p.**: 112°C. **IR** (ATR, cm^{-1}): 3410, 1651, 1645, 1520, 856. **UV-Vis** (DMSO): 316 nm. **^{1}H NMR** (400 MHz, $CDCl_3$): δ=7.33 (dd, $J_{H,H}$=8.4, 2.1 Hz, 1H; Ar-*H*), 7.19 (d, $J_{H,H}$=2.1 Hz, 1H; Ar-*H*), 7.00 (d, $J_{H,H}$=8.4 Hz, 1H; Ar-*H*), 6.62 (d, $J_{H,H}$=2.2 Hz, 1H; H_{pyrone}), 6.17 (dd, $J_{H,H}$=2.0, 0.6 Hz, 1H; H_{pyrone}), 3.95 (s, 3H; OCH_3), 2.37 (d, $J_{H,H}$=0.5 Hz, 3H; CH_3). **^{13}C{^{1}H} NMR** (100 MHz, $CDCl_3$): δ=180.6, 165.4, 164.0, 149.1, 147.2, 123.4, 120.2, 115.2, 114.2, 109.5, 108.2, 56.2, 20.0. **ESI-MS** (HR) *m/z:* $[M+H]^+$ calcd for $C_{13}H_{13}O_4$: 233.0808, found: 233.0812.

2-(3-methoxy-4-(methoxymethoxy)phenyl)-6-methyl-4H-pyran-4-one, 21: To a solution of 2-(4-hydroxy-3-methoxyphenyl)-6-methyl-4H-pyran-4-one **2** (40 mg, 0.17 mmol) in DCM (5 mL) were added DIPEA (67 µL, 0.26 mmol, 1.50 eq.) and MOM chloride (20 µL, 0.38 mmol, 2.21 eq.) under stirring at 0°C. After addition, the flask was sealed and the mixture was stirred for 3h at room temperature (CCM, SiO_2, EtOAc). The reaction mixture was quenched with saturated aqueous NH_4Cl (3 mL) and the organic phase was separated. The aqueous phase was further extracted with DCM (3x5 mL). The combined organic phases were washed with water (3x5 mL) and brine (3x5 mL), then dried over Na_2SO_4, filtered, concentrated, and purified by chromatography (SiO_2, EtOAc) to afford the protected derivative **21** as a white solid (47 mg, 98%). ***R**f*:* 0.30 (EtOAc). **M.p.**: 158°C. **IR** (ATR, cm^{-1}): 1655, 1612, 1512, 858. **UV-Vis** (DMSO): 310 nm. **^{1}H NMR** (400 MHz, $CDCl_3$): δ=7.29 (dd, $J_{H,H}$=8.5, 2.2 Hz, 1H; Ar-*H*), 7.19 (d, $J_{H,H}$=2.1 Hz, 1H; Ar-*H*), 7.17 (d, $J_{H,H}$=8.5 Hz, 1H; Ar-*H*), 6.57 (d, $J_{H,H}$=2.2 Hz, 1H; H_{pyrone}), 6.10 (dd, $J_{H,H}$=2.1, 0.7 Hz, 1H; H_{pyrone}), 5.23 (s, 2H; OCH_2O), 3.89 (s, 3H; OCH_3), 3.47 (s, 3H; OCH_3), 2.32 (d, $J_{H,H}$=0.6 Hz, 3H; CH_3). **^{13}C{^{1}H} NMR** (100 MHz, $CDCl_3$): δ=180.2, 165.2, 163.4, 149.9, 149.2, 125.3, 119.2, 115.9, 114.2, 109.9, 109.0, 95.2, 56.4, 56.1, 19.9. **ESI-MS** (HR) *m/z:* $[M+H]^+$ calcd for $C_{15}H_{17}O_5$: 277.1071, found: 277.1088; *m/z:* $[M+Na]^+$ calcd for $C_{15}H_{16}NaO_5$: 299.0890, found: 299.0899.

(*E*)-2-(3-methoxy-4-(methoxymethoxy)phenyl)-6-(3-methoxy-4-(methoxymethoxy)styryl) -4H-pyran-4-one, 22: A freshly prepared NaOEt solution (1.478 M in EtOH, 2.2 mL, 3.25 mmol, 1.79 eq.) was added dropwise to a mixture of 2-(3-methoxy-4-(methoxymethoxy)phenyl)-6-methyl-4H-pyran-4-one **21** (500 mg, 1.81 mmol) and 3-methoxy-4-(methoxymethoxy) benzaldehyde **3c** (510 mg, 2.59 mmol, 1.43 eq.) in dry EtOH (20 mL) at room temperature. Then the mixture was warmed to 40°C with a heating mantle and stirred for 48h (CCM, SiO_2, EtOAc). The reaction was quenched with water (10 mL) and the crude product was extracted with DCM (4x10 mL). The combined organic phases were washed with water (3x10 mL) and brine (3x10 mL), then dried over Na_2SO_4 and filtered. The concentrated filtrate was purified on column chromatography (SiO_2, EtOAc) to give the title compound **22** as a yellow solid (310 mg, 38%). ***R**f*:* 0.28 (EtOAc). **M.p.**: 131°C. **IR** (ATR, cm^{-1}): 3076, 2932, 1645, 1628, 1599, 1504. **UV-Vis** (DMSO): 356 nm. **^{1}H NMR** (400 MHz, $CDCl_3$): δ=7.46 (dd, $J_{H,H}$=8.5, 2.0 Hz, 1H; Ar-*H*), 7.42 (d, $J_{H,H}$=16.0 Hz, 1H; H_β), 7.31 (d, $J_{H,H}$=1.6 Hz, 1H; Ar-*H*), 7.30 (d, $J_{H,H}$=8.4 Hz, 1H; Ar-*H*), 7.19 (d, $J_{H,H}$=8.1 Hz, 1H; Ar-*H*), 7.09 (m, 2H; Ar-*H*), 6.70 (d, $J_{H,H}$=1.9 Hz, 1H; H_{pyrone}), 6.67 (d, $J_{H,H}$=16.0 Hz, 1H; H_α), 6.31 (d, $J_{H,H}$=1.8 Hz, 1H; H_{pyrone}), 5.32 (s, 2H; OCH_2O), 5.28 (s, 2H; OCH_2O), 3.98 (s, 3H; OCH_3), 3.97 (s, 3H; OCH_3), 3.54 (s,

3H; OCH_3), 3.53 (s, 3H; OCH_3). **^{13}C{^{1}H} NMR** (100 MHz, $CDCl_3$): δ=180.3, 162.8, 161.8, 150.1, 150.0, 149.4, 148.3, 135.8, 129.4, 125.6, 121.7, 119.5, 118.3, 116.1, 116.0, 113.5, 110.5, 109.9, 109.3, 95.3, 95.2, 56.4, 56.1. **ESI-MS** (HR) *m/z:* $[M+H]^+$ calcd for $C_{25}H_{27}O_8$: 455.1700, found: 455.1696; *m/z:* $[M+Na]^+$ calcd for $C_{25}H_{26}NaO_8$: 477.1520, found: 477.1471; *m/z:* $[M+K]^+$ calcd for $C_{25}H_{26}KO_8$: 493.1259, found: 493.1220.

(*E*)-2-(4-hydroxy-3-methoxyphenyl)-6-(4-hydroxy-3-methoxystyryl)-4H-pyran-4-one, 1: To a stirred solution of (E)-2-(3-methoxy-4-(methoxymethoxy)phenyl)-6-(3-methoxy-4-(methoxymethoxy)styryl)-4H-pyran-4-one **22** (170 mg, 0.37 mmol) in MeOH (10 mL) it was added dropwise, at room temperature, an excess of HCl 1M (3 mL, 3.00 mmol, 8.02 eq.). The mixture was then refluxed with a heating mantle for 3h and the reaction advancement was followed by CCM (SiO_2, EtOAc/MeOH, 95:5). At the end, the reaction was quenched with water (10 mL), the precipitated product was filtered, washed with water, and finally dried to afford the 2,6-γ-pyrone **1** as a yellow solid (125 mg, 91%). ***R$_f$***: 0.33 (EtOAc/MeOH, 95:5). **M.p.**: 238 °C. **IR** (ATR, cm^{-1}): 3134 (br), 2932, 1641, 1628, 1595, 1508. **^{1}H NMR** (400 MHz, DMSO-*d6*): δ=9.87 (s, 1H; O*H*), 9.56 (s, 1H; O*H*), 7.58 (dd, $J_{H,H}$=8.3, 2.2 Hz, 1H; Ar-*H*), 7.52 (d, $J_{H,H}$=16.1 Hz, 1H; H_β), 7.52 (d, $J_{H,H}$=2.1 Hz, 1H; Ar-*H*), 7.37 (d, $J_{H,H}$=1.9 Hz, 1H; Ar-*H*), 7.19 (dd, $J_{H,H}$=8.3, 1.9 Hz, 1H; Ar-*H*), 7.01 (d, $J_{H,H}$=16.1 Hz, 1H; H_α), 6.99 (d, $J_{H,H}$=8.3 Hz, 1H; Ar-*H*), 6.86 (d, $J_{H,H}$=7.8 Hz, 1H; Ar-*H*), 6.85 (d, $J_{H,H}$=2.1 Hz, 1H; H_{pyrone}), 6.32 (d, $J_{H,H}$=2.2 Hz, 1H; H_{pyrone}), 3.94 (s, 3H; OCH_3), 3.89 (s, 3H; OCH_3). **^{13}C{^{1}H} NMR** (100 MHz, DMSO-*d6*): δ=180.0, 163.2, 162.6, 151.0, 149.6, 149.0, 148.95, 136.7, 127.7, 123.3, 122.9, 120.7, 117.9, 116.8, 116.6, 113.2, 111.8, 110.7, 109.8, 56.8, 56.7. **ESI-MS** (HR) *m/z:* $[M+H]^+$ calcd for $C_{21}H_{19}O_6$: 367.1176, found: 367.1184; *m/z:* $[M+Na]^+$ calcd for $C_{21}H_{18}NaO_6$: 389.0996, found: 389.0967.

(*Z*)-2-(4-hydroxy-3-methoxyphenyl)-6-(4-hydroxy-3-methoxystyryl)-4H-pyran-4-one, 1': An irradiation at 375 nm of the solution of **1** in DMSO led to **1'** with a ratio: **1/1' 47:53. ^{1}H NMR** (400 MHz, DMSO-*d6*): δ=9.58 (s, 1H; O*H*), 9.36 (s, 1H; O*H*), 7.00 (d, $J_{H,H}$=1.5 Hz, 1H; Ar-*H*), 6.97 (d, $J_{H,H}$=1.9 Hz, 1H; Ar-*H*), 6.94 (d, $J_{H,H}$=12.0 Hz, 1H; H_β), 6.88 (m, 1H; Ar-*H*), 6.83 (d, $J_{H,H}$=2.2 Hz, 1H; H_{pyrone}), 6.80 (dd, $J_{H,H}$=8.4, 2.1 Hz, 1H; Ar-*H*), 6.77 (d, $J_{H,H}$=8.1 Hz, 1H; Ar-*H*), 6.70 (d, $J_{H,H}$=8.4 Hz, 1H; Ar-*H*), 6.33 (d, $J_{H,H}$=2.6 Hz, 1H; H_{pyrone}), 6.32 (d, $J_{H,H}$=12.0 Hz, 1H; H_α), 3.62 (s, 3H; OCH_3), 3.56 (s, 3H; OCH_3). **^{13}C{^{1}H} NMR** (100 MHz, DMSO-*d6*): δ=179.7, 163.3, 162.5, 150.8, 148.6, 148.4, 148.2, 138.7, 127.9, 123.5, 122.3, 120.5, 119.5, 116.3, 116.2, 115.7, 113.7, 110.1, 109.7, 56.3, 56.2. **ESI-MS** (HR) *m/z:* $[M+H]^+$

calcd for $C_{21}H_{19}O_6$: 367.1184, found: 367.1199; *m/z:* $[M+Na]^+$ calcd for $C_{21}H_{18}NaO_6$: 389.0996, found: 389.0967.

Computational methodology

Ground state minima of both isomers of the prepared γ-pyrone analogue of cyclocurcumin **1** was found under the framework of the density functional theory (DFT), applying the B3LYP functional.[46]

To compute the absorption spectra of both isomers, the time-dependent DFT (TD-DFT) was used. Different DFT functionals and basis sets were used to characterize the excitation of the molecule using the Gaussian16 software.[47] As more remarkable, two main behaviors can be shown. The CAM-B3LYP strongly blueshifts the absorption maximum as is common for range-separate functionals.[48] It can be related to an improved representation of charge-transfer states compared to hybrid functionals that avoids the presence of significant intruder states, whose excitation energy would have been artificially lowered. In contrast, B3LYP better describes the shape of the absorption spectrum but yields in the presence of intruder states due to an overstabilization of the S_3 and an increase of the charge transfer states.[46]

To provide UV data more accurate to the one found experimentally, the vibrational and dynamical effects were considered around Franck-Condon region *via* a Wigner distribution, using the NewtonX code to generate 100 structures.[49] Excited states were computed for each one through single point calculations in vacuum at the CAM-B3LYP/6-31G* level of theory considering 20 roots, and finally convoluting all the Gaussian functions resulting from all transition energies and oscillator strengths.[50] Furthermore, this was done for the molecule in different solvents, using the optimized structure and the phase space for each solvent, not the vacuum frequencies. The solvent was included using the polarizable continuum model (PCM)[51] as implemented in Gaussian16,[47] using water, ethanol, dimethyl sulfoxide, and chloroform.

Fluorescence spectrum in vacuo was obtained from a Wigner distribution, sampling the vibrational space on the excited state minimum generating 100 structures. To compute the emission spectra, the first root which represents the S_0 to S_1 transition was only considered.

Coherently with an established protocol[52–55] TPA cross section have been simulated as vertical transition from the ground-state equilibrium geometry only, *i.e.* the Franck-Condon region, and was obtained at TD-DFT level of theory through a quadratic response approach as implemented in DALTON package.[56] CAM-B3LYP exchange-correlation functional and the Pople 6-311++G(d,p) basis set were used, while excitation energies and cross-sections have been calculated considering the effect of water solvent modeled at PCM level.

Steady-state measurements

Absorption and emission spectra. UV-visible spectra were recorded on a Perkin-Elmer Lambda 1050 UV-vis-NIR spectrophotometer using a 1 cm optical path length cell at 25°C, unless otherwise specified. The steady state measurements were recorded on a Jobin Yvon Fluorolog-3 spectrofluorometer from Horiba Scientific and the FluorEssence program. The excitation source was a 450 W xenon lamp, and the detector used was an R-928 operating at a voltage of 950 V. Excitation and emission slits width were 1 nm. The fluorescence quantum yields were determined using quinine sulphate as a standard (Φ = 0.53 in H_2SO_4, 0.05M) using

$$\Phi_x = \Phi_s \left(\frac{Grad_x}{Grad_s}\right)\left(\frac{\eta_x^2}{\eta_s^2}\right)$$

where Φ, Grad and η represent fluorescence quantum yield, gradient from the plot of integrated fluorescence intensity vs. absorbance, and refractive index of the solvent, respectively. The subscripts S and X denote standard and test, respectively.

Kinetics and fatigue resistance. The photo-isomerization was carried out on a 1.0 cm-path-length quartz cell places on a 4-sided cuvette holder (Cuvette Holder with Four Light Ports, CVH100 Thorlabs). Unless otherwise specified, the concentration of the samples was of 40 μM. The kinetics of the photoisomerization process were measured by following the absorption spectrum during irradiation by selected light-emitting diodes (LED), placed perpendicular to the absorbance measurement. To reach the photostationary state of the *E*→*Z* isomerization, the E-stereoisomer was illuminated within the π-π* band using a M375L4.1540 mW LED (LED Power Output 1540mW, 2% power used) with a central wavelength of 375 nm and a bandwidth

(FWHM) of 9 nm. For the reverse transformation, *Z→E* isomerization, the compound was excited within the n-π* band using a M300L4.32 mW LED (LED Power Output: 47mW, full power used) with a central wavelength of 300 nm with a bandwidth (FWHM) of 20 nm. In this case, the concentrations of the compound **22** were of 28.5 μM in DMSO, 33 μM in ethanol, 27 μM in acetonitrile and 24 μM in chloroform. The thermal return process between Z and E isomers was analyzed by measuring the changes of the maximum absorbance wavelength at 25 and 40°C, respectively. Kinetic monitoring of absorbance was performed using an Ocean Optics USB2000 + XR CCD sensor and kinetic constants were determined using "Biokine" software.

Supporting Information. Benchmarking of DFT functionals, experiment procedures and ^{1}H and ^{13}C NMR spectra, physico-chemical characterization of compound **1**, cartesian coordinates of compound **1**.

Acknowledgements

JP acknowledges the French Ministry of Higher Education, Research and Innovation for his PhD grant. The authors greatly acknowledge the NMR Plateforme of Jean Barriol Institut, and MassLor Spectrometry Plateforme of the University of Lorraine. The authors thank F. Dupire for performing mass spectrometry measurements. The authors gratefully acknowledge University of Lorraine, CNRS and the European Regional Development Funds (Programme opérationnel FEDER-FSE Lorraine et Massif des Vosges 2014-2020/"Fire Light" project: "Photo-bio-active molecules and nanoparticles") for financial support.

References

(1) Gozem, S.; Schapiro, I.; Ferre, N.; Olivucci, M. The Molecular Mechanism of Thermal Noise in Rod Photoreceptors. *Science* **2012**, *337* (6099), 1225–1228. https://doi.org/10.1126/science.1220461.

(2) Marazzi, M.; Gattuso, H.; Giussani, A.; Zhang, H.; Navarrete-Miguel, M.; Chipot, C.; Cai, W.; Roca-Sanjuán, D.; Dehez, F.; Monari, A. Induced Night Vision by Singlet-Oxygen-Mediated Activation of Rhodopsin. *J. Phys. Chem. Lett.* **2019**, *10* (22), 7133–7140. https://doi.org/10.1021/acs.jpclett.9b02911.

(3) Sampedro, D.; Migani, A.; Pepi, A.; Busi, E.; Basosi, R.; Latterini, L.; Elisei, F.; Fusi, S.; Ponticelli, F.; Zanirato, V.; Olivucci, M. Design and Photochemical Characterization of a Biomimetic Light-Driven Z / E Switcher. *J. Am. Chem. Soc.* **2004**, *126* (30), 9349–9359. https://doi.org/10.1021/ja038859e.
(4) Bresolí-Obach, R.; Massad, W. A.; Abudulimu, A.; Lüer, L.; Flors, C.; Luis, J. G.; Rosquete, L. I.; Grillo, T. A.; Anamimoghadam, O.; Bucher, G.; Nonell, S. 9-Aryl-Phenalenones: Bioinspired Thermally Reversible Photochromic Compounds for Photoswitching Applications in the Pico-to Milliseconds Range. *Dyes and Pigments* **2021**, *186*, 109060. https://doi.org/10.1016/j.dyepig.2020.109060.
(5) Romero, M. A.; Mateus, P.; Matos, B.; Acuña, Á.; García-Río, L.; Arteaga, J. F.; Pischel, U.; Basílio, N. Binding of Flavylium Ions to Sulfonatocalix[4]Arene and Implication in the Photorelease of Biologically Relevant Guests in Water. *J. Org. Chem.* **2019**, *84* (17), 10852–10859. https://doi.org/10.1021/acs.joc.9b01420.
(6) Marazzi, M.; Francés-Monerris, A.; Mourer, M.; Pasc, A.; Monari, A. Trans-to-Cis Photoisomerization of Cyclocurcumin in Different Environments Rationalized by Computational Photochemistry. *Phys. Chem. Chem. Phys.* **2020**, *22* (8), 4749–4757. https://doi.org/10.1039/C9CP06565B.
(7) Adhikary, R.; Barnes, C. A.; Trampel, R. L.; Wallace, S. J.; Kee, T. W.; Petrich, J. W. Photoinduced Trans-to-Cis Isomerization of Cyclocurcumin. *J. Phys. Chem. B* **2011**, *115* (36), 10707–10714. https://doi.org/10.1021/jp200080s.
(8) Albota, M.; Beljonne, D.; Brédas, J. L.; Ehrlich, J. E.; Fu, J. Y.; Heikal, A. A.; Hess, S. E.; Kogej, T.; Levin, M. D.; Marder, S. R.; McCord-Maughon, D.; Perry, J. W.; Röckel, H.; Rumi, M.; Subramaniam, G.; Webb, W. W.; Wu, X. L.; Xu, C. Design of Organic Molecules with Large Two-Photon Absorption Cross Sections. *Science* **1998**, *281* (5383), 1653–1656. https://doi.org/10.1126/science.281.5383.1653.
(9) Light, R. J.; Hauser, C. R. Aroylations of β-Diketones at the Terminal Methyl Group to Form 1,3,5-Triketones. Cyclizations to 4-Pyrones and 4-Pyridones. *J. Org. Chem.* **1960**, *25* (4), 538–546. https://doi.org/10.1021/jo01074a013.
(10) Knight, J. D.; Metz, C. R.; Beam, C. F.; Pennington, W. T.; VanDerveer, D. G. New Strong Base Synthesis of Symmetrical 1,5-Diaryl-1,3,5-Pentanetriones from Acetone and Benzoate Esters. *Synthetic Commun.* **2008**, *38* (14), 2465–2482. https://doi.org/10.1080/00397910802138488.
(11) Solas, M.; Muñoz, M. A.; Suárez-Pantiga, S.; Sanz, R. Regiodivergent Hydration–Cyclization of Diynones under Gold Catalysis. *Org. Lett.* **2020**, *22* (19), 7681–7687. https://doi.org/10.1021/acs.orglett.0c02892.
(12) Xu, Y.-L.; Teng, Q.-H.; Tong, W.; Wang, H.-S.; Pan, Y.-M.; Ma, X.-L. Atom-Economic Synthesis of 4-Pyrones from Diynones and Water. *Molecules* **2017**, *22* (1), 109. https://doi.org/10.3390/molecules22010109.
(13) Habert, L.; Cariou, K. Photoinduced Aerobic Iodoarene-Catalyzed Spirocyclization of *N* -Oxy-amides to N-Fused Spirolactams. *Angew. Chem.* **2021**, *133* (1), 173–177. https://doi.org/10.1002/ange.202009175.
(14) Li, C.-S.; Lacasse, E. Synthesis of Pyran-4-Ones from Isoxazoles. *Tetrahedron Lett.* **2002**, *43* (19), 3565–3568. https://doi.org/10.1016/S0040-4039(02)00567-1.
(15) Thummala, Y.; Karunakar, G. V.; Doddi, V. R. DBU-Mediated Synthesis of Aryl Acetylenes or 1-Bromoethynylarenes from Aldehydes. *Adv. Synth. Catal.* **2019**, *361* (3), 611–616. https://doi.org/10.1002/adsc.201801334.
(16) Fang, Y.-Q.; Lifchits, O.; Lautens, M. Horner-Wadsworth-Emmons Modification for Ramirez Gem-Dibromoolefination of Aldehydes and Ketones Using P(Oi-Pr)3. *Synlett* **2008**, *2008* (3), 413–417. https://doi.org/10.1055/s-2008-1032045.

(17) 2-(2,2-Dibromoethenyl)-benzenamine. *Org. Synth.* **2009**, *86*, 36–46. https://doi.org/10.15227/orgsyn.086.0036.
(18) Tassano, E.; Alama, A.; Basso, A.; Dondo, G.; Galatini, A.; Riva, R.; Banfi, L. Conjugation of Hydroxytyrosol with Other Natural Phenolic Fragments: From Waste to Antioxidants and Antitumour Compounds: Conjugation of Hydroxytyrosol with Natural Phenolic Fragments. *Eur. J. Org. Chem.* **2015**, *2015* (30), 6710–6726. https://doi.org/10.1002/ejoc.201500931.
(19) Valdomir, G.; Padrón, J.; Padrón, J.; Martín, V.; Davyt, D. Oxazole/Thiazole and Triazole Hybrids Based on α-Amino Acids. *Synthesis* **2014**, *46* (18), 2451–2462. https://doi.org/10.1055/s-0033-1339139.
(20) Morri, A. K.; Thummala, Y.; Doddi, V. R. The Dual Role of 1,8-Diazabicyclo[5.4.0]Undec-7-Ene (DBU) in the Synthesis of Terminal Aryl- and Styryl-Acetylenes via Umpolung Reactivity. *Org. Lett.* **2015**, *17* (18), 4640–4643. https://doi.org/10.1021/acs.orglett.5b02398.
(21) Miyakoshi, T.; Saito, S.; Kumanotani, J. A new synthesis of β-nitro carbonyl compounds from alkyl vinyl ketones with sodium nitrite-acetic acid in tetrahydrofuran. *Chem. Lett.* **1981**, *10* (12), 1677–1678. https://doi.org/10.1246/cl.1981.1677.
(22) Rosini, G.; Ballini, R.; Sorrenti, P. A New Route to 1,4 -Diketones and Its Application to (z)-Jasmone and Dihydrojasmone Synthesis. *Tetrahedron* **1983**, *39* (24), 4127–4132. https://doi.org/10.1016/S0040-4020(01)88632-4.
(23) Mukaiyama, T.; Hoshino, T. The Reactions of Primary Nitroparaffins with Isocyanates [1]. *J. Am. Chem. Soc.* **1960**, *82* (20), 5339–5342. https://doi.org/10.1021/ja01505a017.
(24) Kulandai Raj, A. S.; Kale, B. S.; Mokar, B. D.; Liu, R.-S. Gold-Catalyzed *N* , *O* -Functionalizations of 6-Allenyl-1-Ynes with *N* -Hydroxyanilines To Construct Benzo[*b*]-Azepin-4-One Cores. *Org. Lett.* **2017**, *19* (19), 5340–5343. https://doi.org/10.1021/acs.orglett.7b02629.
(25) Pauli, L.; Tannert, R.; Scheil, R.; Pfaltz, A. Asymmetric Hydrogenation of Furans and Benzofurans with Iridium-Pyridine-Phosphinite Catalysts. *Chem. Eur. J.* **2015**, *21* (4), 1482–1487. https://doi.org/10.1002/chem.201404903.
(26) Rehbein, J.; Leick, S.; Hiersemann, M. Gosteli−Claisen Rearrangement: Substrate Synthesis, Simple Diastereoselectivity, and Kinetic Studies. *J. Org. Chem.* **2009**, *74* (4), 1531–1540. https://doi.org/10.1021/jo802303m.
(27) Persich, P.; Llaveria, J.; Lhermet, R.; de Haro, T.; Stade, R.; Kondoh, A.; Fürstner, A. Increasing the Structural Span of Alkyne Metathesis. *Chem. Eur. J.* **2013**, *19* (39), 13047–13058. https://doi.org/10.1002/chem.201302320.
(28) Zhao, H.-Y.; Wu, F.-S.; Yang, L.; Liang, Y.; Cao, X.-L.; Wang, H.-S.; Pan, Y.-M. Catalyst- and Solvent-Free Approach to 2-Arylated Quinolines *via* [5 + 1] Annulation of 2-Methylquinolines with Diynones. *RSC Adv.* **2018**, *8* (9), 4584–4587. https://doi.org/10.1039/C7RA12716B.
(29) Wang, T.; Shi, S.; Hansmann, M. M.; Rettenmeier, E.; Rudolph, M.; Hashmi, A. S. K. Synthesis of Highly Substituted 3-Formylfurans by a Gold(I)-Catalyzed Oxidation/1,2-Alkynyl Migration/Cyclization Cascade. *Angew. Chem. Int. Ed.* **2014**, *53* (14), 3715–3719. https://doi.org/10.1002/anie.201310146.
(30) Hatano, M.; Sakamoto, T.; Mizuno, T.; Goto, Y.; Ishihara, K. Chiral Supramolecular U-Shaped Catalysts Induce the Multiselective Diels–Alder Reaction of Propargyl Aldehyde. *J. Am. Chem. Soc.* **2018**, *140* (47), 16253–16263. https://doi.org/10.1021/jacs.8b09974.
(31) Zhang, S.; An, B.; Yan, J.; Huang, L.; Li, X. The Synthesis and Evaluation of New Benzophenone Derivatives as Tubulin Polymerization Inhibitors. *RSC Adv.* **2016**, *6* (91), 88453–88462. https://doi.org/10.1039/C6RA16948A.

(32) Pilkington, L. I.; Wagoner, J.; Kline, T.; Polyak, S. J.; Barker, D. 1,4-Benzodioxane Lignans: An Efficient, Asymmetric Synthesis of Flavonolignans and Study of Neolignan Cytotoxicity and Antiviral Profiles. *J. Nat. Prod.* **2018**, *81* (12), 2630–2637. https://doi.org/10.1021/acs.jnatprod.8b00416.
(33) Pang, Y.; An, B.; Lou, L.; Zhang, J.; Yan, J.; Huang, L.; Li, X.; Yin, S. Design, Synthesis, and Biological Evaluation of Novel Selenium-Containing *Iso* Combretastatins and Phenstatins as Antitumor Agents. *J. Med. Chem.* **2017**, *60* (17), 7300–7314. https://doi.org/10.1021/acs.jmedchem.7b00480.
(34) Sakata, Y.; Yasui, E.; Mizukami, M.; Nagumo, S. Cascade Reaction Including a Formal [5 + 2] Cycloaddition by Use of Alkyne-Co2(CO)6 Complex. *Tetrahedron Letters* **2019**, *60* (11), 755–759. https://doi.org/10.1016/j.tetlet.2019.01.045.
(35) Rosiak, A.; Müller, R. M.; Christoffers, J. Synthesis of 2,3-Dihydrothiopyran-4-Ones from 3-Oxo-1-Pentene-4-Ynes. *Monatsh. Chem.* **2007**, *138* (1), 13–26. https://doi.org/10.1007/s00706-006-0571-4.
(36) Tong, W.; Li, Q.-Y.; Xu, Y.-L.; Wang, H.-S.; Chen, Y.-Y.; Pan, Y.-M. An Unexpected Domino Reaction of β-Keto Sulfones with Acetylene Ketones Promoted by Base: Facile Synthesis of 3(2 *H*)-Furanones and Sulfonylbenzenes. *Adv. Synth. Catal.* **2017**, *359* (22), 4025–4035. https://doi.org/10.1002/adsc.201700830.
(37) Xu, Y.-L.; Teng, Q.-H.; Tong, W.; Wang, H.-S.; Pan, Y.-M.; Ma, X.-L. Atom-Economic Synthesis of 4-Pyrones from Diynones and Water. *Molecules* **2017**, *22* (1), 109. https://doi.org/10.3390/molecules22010109.
(38) Ghandi, M.; Bayat, Y.; Teimuri-Mofrad, R. A novel method for the synthesis of formyl and hydroxymethyl derivatives of 4 *h* -pyran-4-one. *Org. Prep. Proced. Int.* **2002**, *34* (5), 525–530. https://doi.org/10.1080/00304940209355774.
(39) Cao, Y.; Chen, L.; Xi, Y.; Li, Y.; Yan, X. Stimuli-Responsive 2,6-Diarylethene-4H-Pyran-4-One Derivatives: Aggregation Induced Emission Enhancement, Mechanochromism and Solvatochromism. *Materials Lett.* **2018**, *212*, 225–230. https://doi.org/10.1016/j.matlet.2017.10.041.
(40) Xia, Y.; Wang, W. Asymmetric Synthesis of Machilin C and Its Analogue. *Chemical Papers* **2010**, *64* (5). https://doi.org/10.2478/s11696-010-0040-8.
(41) Losantos, R.; Pecourneau, J.; Mourer, M.; Parant, S.; Pasc, A.; Monari, A. Trans-Cis Photoisomerization of Biomimetic Cyclocurcumin Analogous Rationalized by Molecular Modelling. *Phys. Chem. Chem. Phys.,* **2021***,* DOI: 10.1039/d1cp01224j.
(42) Pecourneau, J.; Losantos, R.; Monari, A.; Parant, S.; Pasc, A.; Mourer, M. Synthesis and Photoswitching Properties of Bioinspired Dissymmetric γ-Pyrone, Analogue of Cyclocurcumin. *ChemRxiv* **2021**, preprint. https://doi.org/10.26434/chemrxiv.14236454.v1
(43) Faler, C. A.; Joullie, M. M. The Kulinkovich Reaction in the Synthesis of Constrained N,N-Dialkyl Neurotransmitter Analogues. *ChemInform* **2007**, *38* (38). https://doi.org/10.1002/chin.200738058.
(44) Tangdenpaisal, K.; Sualek, S.; Ruchirawat, S.; Ploypradith, P. Factors Affecting Orthogonality in the Deprotection of 2,4-Di-Protected Aromatic Ethers Employing Solid-Supported Acids. *Tetrahedron* **2009**, *65* (22), 4316–4325. https://doi.org/10.1016/j.tet.2009.03.089.
(45) Schmittel, M.; Morbach, G.; Schenk, W. A.; Hagel, M. Synthesis, Thermal Reactivity and Structure of 1,2-Bis(4-Hydroxy-3-Methoxyphenylethynyl)Benzene. *J Chem Crystallogr* **2005**, *35* (5), 373–379. https://doi.org/10.1007/s10870-005-1674-1.
(46) Becke, A. D. Density-functional Thermochemistry. III. The Role of Exact Exchange. *J. Chem. Phys.* **1993**, *98* (7), 5648–5652. https://doi.org/10.1063/1.464913.
(47) Frisch, M. J.; Trucks, G. W.; Schlegel, H. B. **2016**, *Gaussian, Inc.*

(48) Yanai, T.; Tew, D. P.; Handy, N. C. A New Hybrid Exchange–Correlation Functional Using the Coulomb-Attenuating Method (CAM-B3LYP). *Chem. Phys. Lett.* **2004**, *393* (1–3), 51–57. https://doi.org/10.1016/j.cplett.2004.06.011.
(49) Barbatti, M.; Ruckenbauer, M.; Plasser, F.; Pittner, J.; Granucci, G.; Persico, M.; Lischka, H. Newton-X: A Surface-Hopping Program for Nonadiabatic Molecular Dynamics: Newton-X. *WIREs Comput Mol Sci* **2014**, *4* (1), 26–33. https://doi.org/10.1002/wcms.1158.
(50) Hehre, W. J.; Ditchfield, R.; Pople, J. A. Self—Consistent Molecular Orbital Methods. XII. Further Extensions of Gaussian—Type Basis Sets for Use in Molecular Orbital Studies of Organic Molecules. *J. Chem. Phys.* **1972**, *56* (5), 2257–2261. https://doi.org/10.1063/1.1677527.
(51) Tomasi, J.; Mennucci, B.; Cammi, R. Quantum Mechanical Continuum Solvation Models. *Chem. Rev.* **2005**, *105* (8), 2999–3094. https://doi.org/10.1021/cr9904009.
(52) Turan, H. T.; Eken, Y.; Marazzi, M.; Pastore, M.; Aviyente, V.; Monari, A. Assessing One- and Two-Photon Optical Properties of Boron Containing Arenes. *J. Phys. Chem. C* **2016**, *120* (32), 17916–17926. https://doi.org/10.1021/acs.jpcc.6b05493.
(53) Marazzi, M.; Gattuso, H.; Monari, A.; Assfeld, X. Steady-State Linear and Non-Linear Optical Spectroscopy of Organic Chromophores and Bio-Macromolecules. *Front. Chem.* **2018**, *6*, 86. https://doi.org/10.3389/fchem.2018.00086.
(54) Gattuso, H.; Dumont, E.; Marazzi, M.; Monari, A. Two-Photon-Absorption DNA Sensitization via Solvated Electron Production: Unraveling Photochemical Pathways by Molecular Modeling and Simulation. *Phys. Chem. Chem. Phys.* **2016**, *18* (27), 18598–18606. https://doi.org/10.1039/C6CP02592G.
(55) Gattuso, H.; Monari, A.; Marazzi, M. Photophysics of Chlorin E6: From One- and Two-Photon Absorption to Fluorescence and Phosphorescence. *RSC Adv.* **2017**, *7* (18), 10992–10999. https://doi.org/10.1039/C6RA28616J.
(56) Aidas, K.; Angeli, C.; Bak, K. L.; Bakken, V.; Bast, R. *et al.* The Dalton Quantum Chemistry Program System: The Dalton Program. *WIREs Comput Mol Sci* **2014**, *4* (3), 269–284. https://doi.org/10.1002/wcms.1172.